Lappeenranta–Lahti University of Technology LUT
School of Energy Systems
Degree Programme in Electrical Engineering

Ossi Sarmala

BEHAVIOR OF RADIO WAVES IN AN OFFICE ENVIRONMENT

Master's Thesis

Examiners: Prof. Pertti Silventoinen
M.Sc. (Tech.) Heikki Häsä

Supervisors: M.Sc. (Tech.) Heikki Häsä

ABSTRACT

Lappeenranta–Lahti University of Technology LUT
School of Energy Systems
Degree Programme in Electrical Engineering

Ossi Sarmala

BEHAVIOR OF RADIO WAVES IN AN OFFICE ENVIRONMENT

Master's Thesis

2020

65 pages, 21 figures, 3 table, 3 appendices.

Examiners: Prof. Pertti Silventoinen
M.Sc. (Tech.) Heikki Häsä

Keywords: radio waves, radio wave propagation, FDTD, CEM

The uses of radio receivers in offices have become significantly more common in recent years. Due to the proliferation of smart devices in office environments, a comprehensive and broad local area network is required for devices to be able to communicate with each other. In this master's thesis, a simulation environment for simulating radio waves is designed, developed and tested. The simulation environment is based on the FDTD (finite-difference time-domain) method and the office models used in the simulation is based on the office floor plan. The functionality of the simulation was tested by comparing the values of the measurement points obtained at the office with the values obtained from simulation at the same point. The results obtained from the simulation did not correspond to the values obtained from the measurements without processing, after processing the values did not fully correspond to each other, but the values give a rough idea of the radio waves propagation.

TIIVISTELMÄ

Lappeenrannan–Lahden teknillinen yliopisto LUT
School of Energy Systems
Sähkötekniikan koulutusohjelma

Ossi Sarmala

RADIOAALTOJEN KÄYTTÄYTYMINEN TOIMISTOYMPÄRISTÖSSÄ

Diplomityö

2020

65 sivua, 21 kuvaa, 3 taulukkoa, 3 liitettä.

Tarkastajat: Prof. Pertti Silventoinen
DI Heikki Häsä

Hakusanat: radioaallot, radioaaltojen eteneminen, FDTD, CEM

Radiovastaanottimien käyttö on yleistynyt toimistoissa merkittävästi viimeisten vuosien aikana. Älylaitteiden yleistymisen takia toimistoympäristöissä vaaditaan kattava ja laaja lähiverkko, jotta laitteet pystyisivät kommunikoimaan keskenään. Tässä diplomityössä suunnitellaan, kehitetään ja testataan radioaaltojen simuloimiseen tarkoitettu simulointiympäristö. Simulaatioympäristö perustuu FDTD menetelmään ja simulaatiossa käytetty toimiston malli perustuvat toimiston pohjapiirustukseen. Simulaation toimivuutta testattiin vertaamalla toimistolla saatujen mittauspisteiden arvoja samasta pisteestä saatuihin simulaation arvoihin. Simulaatiosta saadut tulokset eivät vastanneet mittauksista saatuja arvoja ilman prosessointi, prosessoinnin jälkeen arvot eivät vastanneet täysin toisiaan, mutta arvojen perusteella saadaan karkea mielikuva radioaaltojen etenemisestä.

PREFACE

First of all, I would like to thank the examiners of this thesis. Thank you professor Silventoinen for the support and feedback during the thesis. Thank you Heikki and Pasi for for supporting and for helping with the thesis, especially when the simulation did not want to progress. Thanks also to the Research Foundation of LUT, which made it possible to make the thesis during these difficult times.

To my friends: Thank you J-P, Krister, Matti and Sakari and all of my other friends for your support, these years have been the best of my life. Thank you for being apart of my journey.

To my family: Thank you for all your support over these years. I'm so grateful to have a family like you. Thanks for always being there. Special thanks to my brother Lauri, who helps with the thesis by telling enthusiastically about Finnish office construction.

Joensuu, December 7, 2020

Ossi Sarmala

CONTENTS

LIST OF ABBREVIATIONS & SYMBOLS

Abbreviations

CAD	Computer-aided Design
CFL	Courant-Friedrichs-Lewy
CEM	Computational electromagnetics
FDTD	Finite-Difference Time-Domain
IEEE	Institute of Electrical and Electronics Engineers
IR	Infrared
ISM	Industrial, Science and Medical
ITU	International Telecommunication Union
PML	Perfectly Matched Layer
RAM	Random Access Memory
RSSI	Received Signal Strength Indication
RX	Receive
TX	Transmit
UPML	Uniaxial Perfectly Matched Layer
Wi-Fi	Wireless Fidelity

Symbols

α	Attenuation constant
$\mathbf{B}$	Magnetic flux density vector $\left[\frac{\mathrm{Wb}}{\mathrm{m}^2}\right]$
c	Speed of light $\left[299792458\frac{\mathrm{m}}{\mathrm{s}}\right]$
$\mathbf{D}$	Electric flux density vector $\left[\frac{\mathrm{C}}{\mathrm{m}^2}\right]$
δ	Skin depth $[\mathrm{m}]$
$\mathbf{E}$	Electric field strength vector $\left[\frac{\mathrm{V}}{\mathrm{m}}\right]$
ϵ	Permittivity $\left[\frac{\mathrm{F}}{\mathrm{m}}\right]$
ϵ_0	Vacuum permittivity $\left[8.854187\frac{\mathrm{pF}}{\mathrm{m}}\right]$
ϵ_r	Relative permittivity
$\mathbf{H}$	Magnetic field strength vector $\left[\frac{\mathrm{A}}{\mathrm{m}}\right]$
$\mathbf{J}$	Eletric current density vector $\left[\frac{\mathrm{A}}{\mathrm{m}^2}\right]$
$\mathbf{M}$	Magnetic current density vector $\left[\frac{\mathrm{V}}{\mathrm{m}^2}\right]$
μ	Permeablity $\left[\frac{\mathrm{H}}{\mathrm{m}}\right]$
μ_0	Vacuum permeability $\left[1.256763\frac{\mu\mathrm{H}}{\mathrm{m}}\right]$
μ_r	Relative permeablity
n	Refractive index
ω	Angular velocity $[\mathrm{s}^{-1}]$
ρ_e	Electric charge density $\left[\frac{\mathrm{C}}{\mathrm{m}^3}\right]$
ρ_m	Magnetic charge density $\left[\frac{\mathrm{Wb}}{\mathrm{m}^3}\right]$
σ	Conductivity $\left[\frac{\mathrm{S}}{\mathrm{m}}\right]$

1 INTRODUCTION

Devices operating in the 2.4 GHz frequency range have become more common in offices and households. Due to the proliferation of smart devices, the design and construction of comprehensive local networks requires a lot of time for the network to function properly. Maintaining a stable connection between smart devices is important in some cases, such as security and control systems.

1.1 Background

Mobile device usage in offices have increase recently, because mobility and versatility of devices. Almost every smart device requires a constant Internet access to get the most out of the device. For this reason, offices require a very comprehensive and broad local area network. The layout of Wi-Fi (Wireless Fidelity) access points requires design so that the access points do not interfere with each other and provide the broadest possible network cover for the devices. Illustrating radio waves is relatively challenging for humans because radio waves may be reflected from surfaces or propagate to material. For this reason, radio wave simulation is the best solution to illustrate the propagation of radio waves in offices.

1.2 Objectives and delimitations

The objective of this thesis is to design a simulation environments that can be used to simulate the propagation of radio waves in office environment. The results obtained from the simulation environment should correspond to the values measured in the office.

The objective is also to create a relatively accurate model of the office and the model should be able to be utilized in the simulation. The office model should be easy to model, either in old or new buildings, for example by using floor plans of the office.

The thesis is limited to studying only one frequency (2.4GHz), the limited frequency has been chosen because frequency range is generally used in smart devices. Simulating other frequencies is also possible in a simulation environment, but the 2.4 GHz frequency is commonly used in smartphones and other Bluetooth and Wi-Fi devices.

The thesis also limits the number of methods used in the simulation to only cover one method, because the purpose of the thesis is to find a suitable simulation environment. In the development of two or more simulation environments, resources would be shared among the simulation environments, while with one simulation method could focus on improving simulation environment.

1.3 Structure of the thesis

This thesis is divided into eight chapters. First, in chapter 1, the background and objectives of the thesis. Then, in chapter 2, the basis of radio waves, from how radio waves are formed to definition of radio waves. In chapter 3, the behavior of radio waves. Chapter 3 reviews the basis of electromagnetism, from composition to Maxwell's equations. The chapter also reviews the behavior of radio waves with materials. Chapter 4 reviews the foundations of the Computational Electromagnetics (CEM) method used in the thesis. In chapter 5, the simulation environment created for the thesis and the limitations associated with it are discussed. Chapter 6 reviews things to consider when modeling an office and performing measurements. Chapter 7 reviews the results of the simulation and measurement. The chapter compares the results obtained and assesses what the differences might be due to. Chapter 8 provides a summary of the thesis.

2 RADIO WAVES

Radio waves are part of the electromagnetic spectrum, the definition of radio wave frequency range varies greatly, but in general the frequency range of radio waves can be considered from 3 Hz to 300 GHz. Radio waves have the lowest frequency in the electromagnetic spectrum and radio waves are located before infrared radiation (IR). Radio waves have lower frequency and longer wavelength than infrared radiation. Figure 1 shows the spectrum of electromagnetic radiation up to X-ray frequencies, where the frequency of radiation increases from right to left. The radio frequencies are located from the right edge of the figure to the right edge of the infrared radiation.

Radio waves are radiation formed by the acceleration of charged particles. The energy released in the radiation consists of the kinetic energy of the particles, as a result, a radiation particle accelerates less than a neutral particle of the same mass. [1]

Radio waves can be generated by alternating current, in electrical devices radio waves are generated by a transmitter. The transmitter acts as a current supply that supplies alternating current to the antenna at the desired frequency.

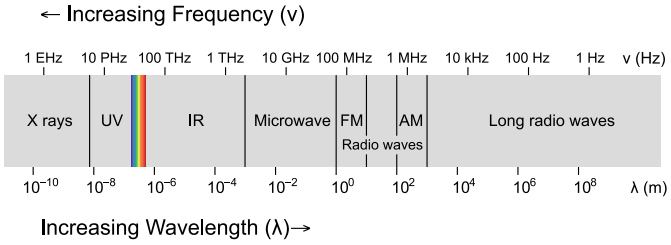

Figure 1. Radio frequency spectrum. Figure is retrieved from [2] and modified under the CC BY-SA 3.0 license.

The International Telecommunication Union (ITU) divides the radio spectrum into 12 bands with frequencies ranging from 3 Hz to 300 GHz (also including infrared band (300-3000 GHz)) [3]. Table 1 shows the ITU defined frequency bands and their frequency range. Institute of Electrical and Electronics Engineers (IEEE) divides the radio spectrum into 14 radar-frequency bands ranging from 3 MHz to 1000 GHz [4].

In Finland, a more precise allocation of radio frequencies is based on the ITU Radio Regulations (RR) and the European Radiocommunications Committee (ERC) Report [5].

Table 1. ITU Frequency bands and frequencies

Band number	Frequency range
1	3 - 30 Hz
2	30 - 300 Hz
3	300 - 3000 Hz
4	3 - 3 kHz
5	30 - 300 kHz
6	300 - 3000 kHz
7	3 - 300 MHz
8	30 - 300 MHz
9	300 - 3000 MHz
10	3 - 30 GHz
11	30 - 300 GHz
12	300 - 3000 GHz

From figure 1 can be observed that frequency band 12 is located in the far-infrared region. This frequency band can be used for example in radio astronomy.

2.1 ISM band

ISM bands are frequency bands for industrial, scientific and medical use (ISM), the frequency band can be used for other communications in addition to those mentioned above. The ISM band is designed to be used to receive and transmit local radio frequencies [6]. The use of the band does not require a separate permit, the devices operating in the band have the highest transmission power restrictions. Due to the free use of bands, several different communication protocols operate in the frequency band, and in household appliances intended for consumer use, the ISM band is used, for example in microwave ovens. Table 2 lists all ISM bands defined by the ITU:

Table 2. ISM bands [6]

Frequency range	Centre frequency
6.765 - 6.795 MHz	6.780 MHz
13.553 - 13.567 MHz	13.560 MHz
26.957 - 27.283 MHz	27.120 MHz
40.66 - 40.70 MHz	40.68 MHz
433.05 - 434.79 MHz	433.92 MHz
902 - 928 MHz	915 MHz
2.40 - 2.50 GHz	2.45 GHz
5.725 - 5.875 GHz	5.800 GHz
24.0 - 24.25 GHz	24.125 GHz
61 - 61.5 GHz	61.25 GHz
122 - 123 GHz	122.5 GHz
244 - 246 GHz	245 GHz

One of the most common frequency bands for consumer use is 2.4-2.5 GHz. The band is used by Wi-Fi, Bluetooth and Zigbee protocols, for example. The band is also commonly used in microwave ovens. Microwave ovens with defective or poor shielding may emit a highly "dirty" signal throughout the 2.4 GHz band, which may cause interference to other devices operating on the same frequency.

3 BEHAVIOR OF RADIO WAVES

In this chapter composition of radio waves and behavior of radio waves are examined. As part of electromagnetic radiation, radio waves behave in the same way as other electromagnetic waves.

As radio waves encounter materials, their behavior changes. Radio waves may be reflected or propagated into the material. Within materials, the properties of radio waves change, for example, the propagation speed, either increases or decreases depending on the properties of the material.

3.1 Composition of radio waves

Electromagnetic radiation consists of electric and magnetic fields. The fields are in phase, but the fields are perpendicular to each other and perpendicular to the direction of propagation. Figure 2 shows an electromagnetic wave, the direction of propagation of the wave is parallel to the y-axis. In the figure, the electric field is depicted in blue and the magnetic field in red.

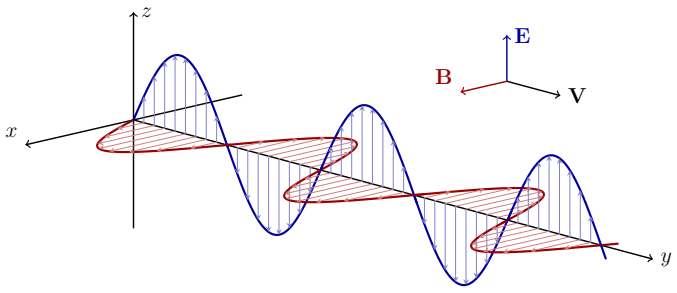

Figure 2. Electromagnetic wave

According to Ampère – Maxwell's law (1a), a variable electric field induces a magnetic field, and correspondingly, according to Maxwell-Faraday's law (1b), a variable magnetic field induces an electric field [1].

3.2 Maxwell's equations

Maxwell's equations are a collection of equations that serve as the basis for classical electromagnetism. Maxwell's equations are named after James Clerk Maxwell (1831-1879), who published the first versions of the equations in 1861 in the paper "On Physical Lines of Forces" [7]. In 1864, Maxwell published paper called "A Dynamical Theory of the Electromagnetic Field" where he proposed that light is an electromagnetic phenomenon [8]. In the same paper, he presented 20 equations involving 20 variables that mathematically represent everything that was known about electricity and magnetism [8] [9]. In 1884 Oliver Heaviside (1850-1925) rewrote Maxwell's equations to correspond to modern vector terminology, he reduced Maxwell's equations to correspond to four vector equations in two variables [10]. These four equations are today known as Maxwell's equations.

$$\nabla \times \mathbf{H} = \frac{\partial \mathbf{D}}{\partial t} + \mathbf{J} \tag{1a}$$

$$\nabla \times \mathbf{E} = -\frac{\partial \mathbf{B}}{\partial t} - \mathbf{M} \tag{1b}$$

$$\nabla \cdot \mathbf{D} = \rho_{\mathrm{e}} \tag{1c}$$

$$\nabla \cdot \mathbf{B} = \rho_{\mathrm{m}} \tag{1d}$$

where $\mathbf{H}$ is the magnetic field strength, $\mathbf{D}$ is the electric flux density, $\mathbf{J}$ is the electric current density, $\mathbf{E}$ is the electric field strength, $\mathbf{B}$ is the magnetic flux density, $\mathbf{M}$ is the magnetic current density, ρ_{e} is the electric charge density and ρ_{m} is the magnetic charge density. $\mathbf{M}$ and ρ_{m} are usually zeros [1].

The electric current density $\mathbf{J}$ consist of two components, the conduction electric current density $\mathbf{J}_{\mathrm{c}} = \sigma^{\mathrm{e}}\mathbf{E}$ and the impressed current density $\mathbf{J}_{\mathrm{i}}$. Also the magnetic current density $\mathbf{M}$ consist of two components, the conduction magnetic current density $\mathbf{M}_{\mathrm{c}} = \sigma^{\mathrm{m}}\mathbf{H}$ and the impressed magnetic current density $\mathbf{M}_{\mathrm{i}}$.

$$\mathbf{J} = \sigma^{\mathrm{e}}\mathbf{E} + \mathbf{J}_{\mathrm{i}} \tag{2a}$$

$$\mathbf{M} = \sigma^{\mathrm{m}}\mathbf{H} + \mathbf{M}_{\mathrm{i}} \tag{2b}$$

Electric flux density **D** and magnetic flux density **B** relate to electric field strength **E** and magnetic current density **H** using simple proportions:

$$\mathbf{D} = \epsilon\mathbf{E} = \epsilon_{\mathrm{r}}\epsilon_0\mathbf{E} \tag{3a}$$

$$\mathbf{B} = \mu\mathbf{H} = \mu_{\mathrm{r}}\mu_0\mathbf{H} \tag{3b}$$

where ϵ_{r} is relative permittivity, μ_{r} is relative permability and ϵ_0 and μ_0 are free space permittivity and permeability, respectively.

Equations (2) and (3) can be substitute into Maxwell's equations (1)

$$\nabla \times \mathbf{H} = \epsilon\frac{\partial\mathbf{E}}{\partial t} + \sigma^{\mathrm{e}}\mathbf{E} + \mathbf{J}_{\mathrm{i}} \tag{4a}$$

$$\nabla \times \mathbf{E} = -\mu\frac{\partial\mathbf{H}}{\partial t} - \sigma^{\mathrm{m}}\mathbf{H} - \mathbf{M}_{\mathrm{i}} \tag{4b}$$

In the thesis the values of **M** and ρ_{m} are assumed to be zero everywhere. The existence of these values would require a magnetic monopoly, which is currently a hypothetical elementary particle which existence in nature has not yet been observed [11].

3.3 Radio wave propagation speed

The propagation speed of radio waves depends on the material where the wave propagates. In the vacuum, radio waves travel at the speed of light. As radio waves move from one material to another, the speed of propagation of radio waves must also change, changes in speed can be calculated using Snell's law. In Snell's law, the ratio of the incidence and refraction angles of the waves is the same as the ratio of propagation speeds and refractive indices [12].

$$\frac{\sin\theta_{\mathrm{t}}}{\sin\theta_{\mathrm{i}}} = \frac{v_2}{v_1} = \frac{n_1}{n_2} \tag{5}$$

where θ_{t} is refraction angle, θ_{i} is incidence angle, v is propagation speed of wave and n is

refractive index of material.

In law of reflection, rays reflected from the surface of the material, the angle of reflected ray to the normal is equal to the angle of incident to the normal [1].

$$\sin\theta_{\mathrm{i}} = \sin\theta_{\mathrm{r}} \tag{6}$$

Figure 3 shows Snell's law, in the figure rays are moving from left to right. Rays are moving from material with the lower refractive index to material with the high refractive index. Normal to the surface is marked as dotted line. In figure angles θ_{i} and θ_{r} are equal to the normal. The angle θ_{t} is gently then the angle θ_{i} due to differences in refractive indexes.

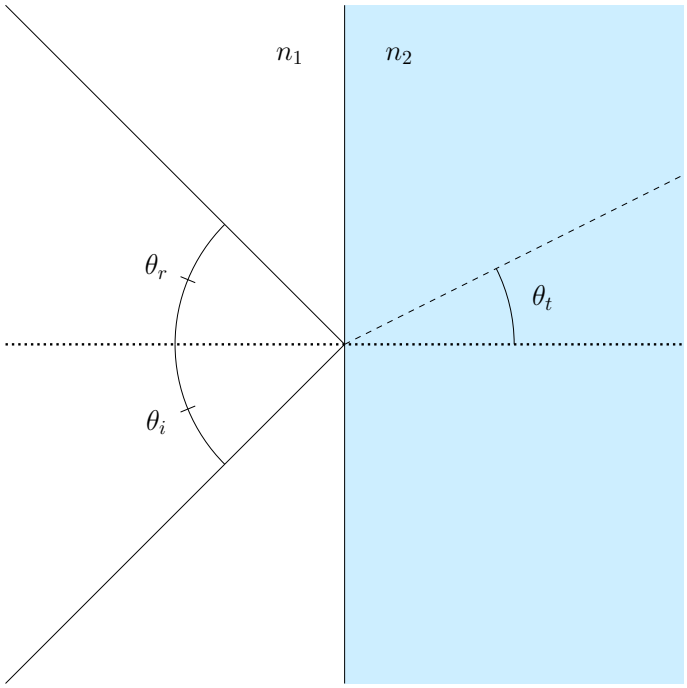

Figure 3. Snell's law

In a vacuum, radio waves propagate at a speed of light c, and in a material, the speed at which a radio wave propagates depends on the permittivity and permeability of the material [13].

$$v = \frac{1}{\sqrt{\mu\epsilon}} \tag{7}$$

The values of permeability and permeability can be expressed by relative values, where the rate of propagation of radio waves depends on the coefficient of the speed of light [13].

$$v = \frac{1}{\sqrt{\mu_{\mathrm{r}}\epsilon_{\mathrm{r}}}\sqrt{\mu_0\epsilon_0}} = \frac{1}{\sqrt{\mu_{\mathrm{r}}\epsilon_{\mathrm{r}}}}c \tag{8}$$

From Equation 8, it can be seen that the speed of propagation in a vacuum is the speed of light and in a material the speed of propagation slows down as the relative permittivity and permeability increase.

As the waves move from one material to another, the propagation speed of the waves changes, and as a result, the wavelength of the waves also changes. As the wavefront moves into the material, the speed of the front decelerates or accelerates depending on the differences in the properties of the materials. The velocities of the waves following the wavefront remain the same until the wave travels to the material, as the waves move at different velocities in different materials this causes the waves to compress, i.e. the wavelength of the wave to change.

3.4 Absorption of radio waves in materials

The most important properties of materials in the absorption of electromagnetic waves are the permeability, permeability and conductivity of the material. The electric field of a wave is affected by permittivity and conductivity and the magnetic field by permeability [1].

For most materials, the permeability is almost the same as the vacuum permeability, i.e., the relative permeability is close to one. For diamagnetic and paramagnetic materials, the relative permeability is lower and higher, respectively. [1]

As shown in equation 3a the relationship between electric flux density and electric field strength depends on the material permittivity. The permittivity in the equation is actually complex [1]. The equation can be rewritten in the form:

$$\mathbf{D}(\omega) = \hat{\epsilon}(\omega)\mathbf{E}(\omega) \tag{9}$$

where $\hat{\varepsilon}$ is complex permittivity, which is obtained by the equation:

$$\hat{\epsilon}(\omega) = \epsilon_0 \left(\epsilon_\mathrm{r} + \frac{\sigma}{j\omega\epsilon_0} \right) \tag{10}$$

where ϵ_r is relative permittivity, ϵ_0 is permittivity of free space, σ is conductivite of the material and ω is angular velocity of wave.

3.4.1 Skin depth

Skin depth describes you how deep the wave can penetrate the surface of the material until the wave is attenuated to e^{-1} from the original wave [13]. The attenuated wave amplitude is about 37$\%$ of the original wave.

In order to calculate the attenuation in a material, it is necessary to know the attenuation constant of the material, the constant is given by the equation:

$$\alpha = \omega \sqrt{\frac{\epsilon_\mathrm{r}\epsilon_0\mu_\mathrm{r}\mu_0}{2}} \sqrt{\sqrt{1 + \left(\frac{\sigma}{\epsilon_\mathrm{r}\epsilon_0\omega} \right)^2} - 1} \tag{11}$$

where ω is angular velocity of wave, σ, ϵ_r ja μ_r are material conductivity, relative permittivity and relative permeability, respectively.

Attenuation constant can be defined by the amplitude ratio.

$$\left| \frac{A_0}{A_\delta} \right| = e^{\alpha\delta} \tag{12}$$

where A_δ is amplitude of penetrating wave at depth of δ and A_0 is wave amplitude on the surface.

When calculating skin depth, it is known that at skin depth the amplitude of the wave is e^{-1}. Amplitude value at skin depth (e^{-1}) can be placed into equation 12, than the amplitude ratio for skin depth can be calculated.

$$\left|\frac{A_0}{A_\delta}\right| = \left|\frac{1}{e^{-1}}\right| = e \tag{13}$$

By placing equation 13 into equation 12, the skin depth equation is obtained. By placing the material values in Equation 11 and placing attenuation constant into skin depth equation, the skin effect depth can be calculated.

$$\delta = \frac{1}{\alpha} = \frac{1}{\omega\sqrt{\frac{\epsilon\mu}{2}}\sqrt{\sqrt{1+\left(\frac{\sigma}{\epsilon\omega}\right)^2}-1}} \tag{14}$$

Table 3 shows the skin depth values for couple of the most common building materials. The values in the table are directional, the values of the materials can fluctuate significantly depending on, for example, moisture level.

Table 3. Common building materials skin depth at 2.4GHz.

Material	σ (S/m)	ϵ_r	μ_r	δ at 2.4 GHz (cm)	
Air	0	1	1	∞	[14], [1]
Concreate	0.066	5.310	1	3.992	[14]
Wood	0.012	1.990	1	9.374	[14]
Glass	0.012	6.270	1	9.296	[14]
Plaster board	0.05	2.3	1	16.155	[15]
Metal	10^7	1	100	0.0178	[14], [16]

3.5 Radio wave reflection and transmission in material

The amount of reflectance and transmittance of waves can be calculated by using Fresnel equations. Fresnel equations give the amount of reflectance and transmittance as a ratio to the original wave. The values of reflectance and transmittance depend on the polarization of the wave, in Fresnel equations (15) the terms r_s and t_s correspond to the perpendicularly polarized wave and the terms r_p and t_p to the parallel polarized wave. [12]

$$r_{\mathrm{s}} = \frac{E_{\mathrm{t}}}{E_{\mathrm{i}}} = \frac{n_1 \cos\theta_{\mathrm{i}} - n_2 \cos\theta_{\mathrm{t}}}{n_1 \cos\theta_{\mathrm{i}} + n_2 \cos\theta_{\mathrm{t}}} \tag{15a}$$

$$t_{\mathrm{s}} = \frac{E_{\mathrm{r}}}{E_{\mathrm{i}}} = \frac{2n_1 \cos\theta_{\mathrm{i}}}{n_1 \cos\theta_{\mathrm{i}} + n_2 \cos\theta_{\mathrm{t}}} \tag{15b}$$

$$r_{\mathrm{p}} = \frac{E_{\mathrm{t}}}{E_{\mathrm{i}}} = \frac{n_2 \cos\theta_{\mathrm{i}} - n_1 \cos\theta_{\mathrm{t}}}{n_2 \cos\theta_{\mathrm{i}} + n_1 \cos\theta_{\mathrm{t}}} \tag{15c}$$

$$t_{\mathrm{p}} = \frac{E_{\mathrm{r}}}{E_{\mathrm{i}}} = \frac{2n_1 \cos\theta_{\mathrm{i}}}{n_2 \cos\theta_{\mathrm{i}} + n_1 \cos\theta_{\mathrm{t}}} \tag{15d}$$

where n_1 and n_2 are material refractive indexes and θ_{i} and θ_{t} are incident and refraction angles, respectively.

The refractive indices of the material can be expressed with relative permittivity and permeability [12]:

$$n = \sqrt{\epsilon_{\mathrm{r}} \mu_{\mathrm{r}}} \tag{16}$$

By placing equation 16 into equations 15, it can be seen that the reflectance and transmittance of the waves depend on the properties of the material and the angle of incidence of the waves.

4 FINITE-DIFFERENCE TIME-DOMAIN

FDTD (Finite-difference time-domain) algorithm is popular tool to solving Maxwell's equations. In FDTD simulation space is divided into the space grid these square voxels (also known as cells) are updated based on past electric- and magnetic fields with update equations. FDTD can be used for many purposes, such as antenna pattern modeling, radar reflection modeling, and microwave devices [17].

4.1 The Yee algorithm

The Yee algorithm is FDTD algorithm where Maxwell's equations are replaced by finite-difference equation, the algorithm was first proposed by Kane S. Yee in 1966 [18]. In the Yee algorithm Ampère – Maxwell's (1a) and Farday – Maxwell's laws (1b) derivatives are placed with finite-differences, and electric and magnetic fields are staggered in space and time [19]. This staggering allows fields to be updated based on previous and adjacent field values.

For example, electric field vectors are located at integer steps and magnetic field vectors are located between electric field vectors, and in time electric fields are updated at integer time steps and magnetic fields are update between electric fields. In figure 4 electric- and magnetic field are staggered according to the Yee algorithm.

Advantages for using Yee grid compared to collocated grid are [20]:

1. Grid have divergence-free nature, $\nabla \cdot (\epsilon \mathbf{E}) = 0$ and $\nabla \cdot (\mu \mathbf{H}) = 0$
2. Physical boundaries are naturally maintained, special boundary conditions are not required at the interface.
3. Curl equations are central-difference and second-order accurate.

Figure 4 presents 2D and 3D cells with electric and magnetic vectors. In 1D-grid only two vectors are required Ey and Hx or Ex and Hy, in 2D-grid three vectors are required Ez, Hx and Hy (tranverse magnetic mode (TM-mode)) or Hz, Ex and Ey (tranverse electic mode (TE-mode)) and in 3D-grid all six vectors are required Hz, Hx, Hy, Ez, Ey and Ex.

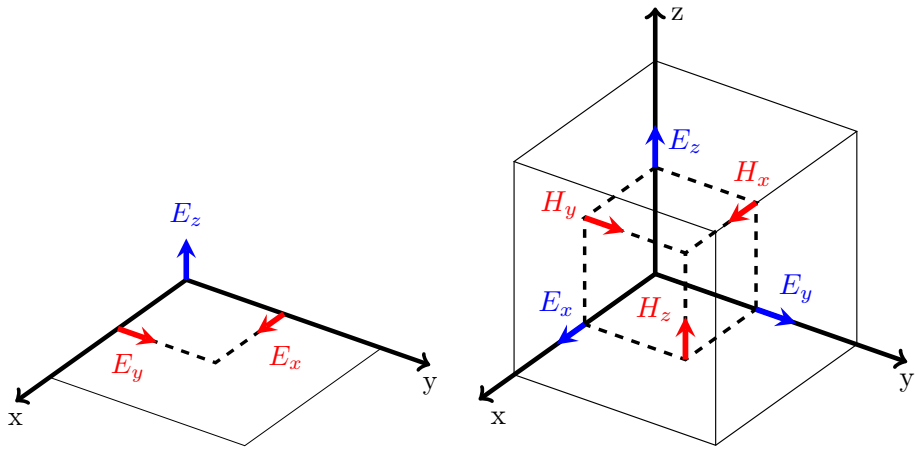

(a) TE-mode (b)

Figure 4. Yee-grids: (a) Two dimension plane, transverse electric mode; (b) Three dimension voxel

In the Yee-grid Ampere's (1a) and Faraday's (1b) laws derivatives are approximated with finite-difference method.

$$\frac{\partial \mathbf{E}}{\partial t} = \frac{1}{\epsilon}\nabla \times \mathbf{H} - \frac{1}{\epsilon}(\sigma^m \mathbf{E} + \mathbf{J}_i) \tag{17a}$$

$$\frac{\partial \mathbf{H}}{\partial t} = -\frac{1}{\mu}\nabla \times \mathbf{E} - \frac{1}{\mu}(\sigma^e \mathbf{H} + \mathbf{M}_i) \tag{17b}$$

From equations 17, electric- and magnetic field vectors can be divided to x, y and z components. For example E_x component can be expressed as:

$$\frac{\partial E_x}{\partial t} = \frac{1}{\epsilon_x}\left[\frac{\partial H_z}{\partial y} - \frac{\partial H_y}{\partial z} - J_{ix} - \sigma^e E_x\right] \tag{18}$$

In equation 18, partial derivatives can be rewritten with finite-difference approximation.

$$\begin{aligned}\frac{E_x^{n+1}(i,j,k)-E_x^n(i,j,k)}{\Delta t} =& \frac{1}{\varepsilon_x(i,j,k)}\frac{H_z^{n+\frac{1}{2}}(i,j,k)-H_z^{n+\frac{1}{2}}(i,j-1,k)}{\Delta y} \\ &- \frac{1}{\varepsilon_x(i,j,k)}\frac{H_y^{n+\frac{1}{2}}(i,j,k)-H_y^{n+\frac{1}{2}}(i,j,k-1)}{\Delta z} \\ &- \frac{\sigma_x^e(i,j,k)}{\varepsilon_x(i,j,k)}E_x^{n+\frac{1}{2}}(i,j,k) - \frac{1}{\varepsilon_x(i,j,k)}J_{ix}^{n+\frac{1}{2}}(i,j,k)\end{aligned} \tag{19}$$

In equation 19, $E_x^{n+1/2}$ is required in calculation but electric field components are only defined at integer time steps. Term $E_x^{n+1/2}$ can be approximated with semi-implicit method. In semi-implicit method electric field terms (n+1) and (n) are averaged as shown in equation 20.

$$E_x^{n+\frac{1}{2}}(i,j,k) = \frac{E_x^{n+1}(i,j,k)+E_x^n(i,j,k)}{2} \tag{20}$$

Equation 20 can be substitute into equation 19. Term E_x^{n+1} is kept on the left side and other terms are moved to the right side. On the right side common factor can be taken, update equations for E_{x} and H_{x} can be written as

$$\begin{aligned}E_{\mathrm{x}}^{n+1}(i,j,k) =& C_{\mathrm{exe}}(i,j,k)\times E_x^n(i,j,k) \\ &+ C_{\mathrm{exhz}}(i,j,k)\times\left(H_z^{n+\frac{1}{2}}(i,j,k)-H_z^{n+\frac{1}{2}}(i,j-1,k)\right) \\ &+ C_{\mathrm{exhy}}(i,j,k)\times\left(H_y^{n+\frac{1}{2}}(i,j,k)-H_y^{n+\frac{1}{2}}(i,j,k-1)\right) \\ &+ C_{\mathrm{exj}}(i,j,k)\times J_{ix}^{n+\frac{1}{2}}(i,j,k)\end{aligned} \tag{21}$$

where C_{exe}, C_{exhz}, C_{exhy} and C_{exj} are

$$C_{\text{exe}}(i,j,k) = \frac{2\varepsilon_x(i,j,k) - \Delta t\sigma_x^e(i,j,k)}{2\varepsilon_x(i,j,k) + \Delta t\sigma_x^e(i,j,k)} \tag{22a}$$

$$C_{\text{exhz}}(i,j,k) = \frac{2\Delta t}{(2\varepsilon_x(i,j,k) + \Delta t\sigma_x^e(i,j,k))\,\Delta y} \tag{22b}$$

$$C_{\text{exhy}}(i,j,k) = -\frac{2\Delta t}{(2\varepsilon_x(i,j,k) + \Delta t\sigma_x^e(i,j,k))\,\Delta z} \tag{22c}$$

$$C_{\text{exj}}(i,j,k) = -\frac{2\Delta t}{2\varepsilon_x(i,j,k) + \Delta t\sigma_x^e(i,j,k)} \tag{22d}$$

$$\begin{aligned} H_{\text{x}}^{n+\frac{1}{2}}(i,j,k) =& C_{\text{hxh}}(i,j,k) \times H_{\text{x}}^{n-\frac{1}{2}}(i,j,k) \\ &+ C_{\text{hxey}}(i,j,k) \times \left(E_{\text{y}}^n(i,j,k+1) - E_{\text{y}}^n(i,j,k)\right) \\ &+ C_{\text{hxez}}(i,j,k) \times (E_{\text{z}}^n(i,j+1,k) - E_{\text{z}}^n(i,j,k)) \\ &+ C_{\text{hxm}}(i,j,k) \times M_{\text{ix}}^n(i,j,k) \end{aligned} \tag{23}$$

where C_{hxh}, C_{hxey}, C_{hxez}, and C_{hxm} are

$$C_{\text{hxh}}(i,j,k) = \frac{2\mu_x(i,j,k) - \Delta t\sigma_x^m(i,j,k)}{2\mu_x(i,j,k) + \Delta t\sigma_x^m(i,j,k)} \tag{24a}$$

$$C_{\text{hxey}}(i,j,k) = \frac{2\Delta t}{(2\mu_x(i,j,k) + \Delta t\sigma_x^m(i,j,k))\,\Delta z} \tag{24b}$$

$$C_{\text{hxez}}(i,j,k) = -\frac{2\Delta t}{(2\mu_x(i,j,k) + \Delta t\sigma_x^m(i,j,k))\,\Delta y} \tag{24c}$$

$$C_{\text{hxm}}(i,j,k) = -\frac{2\Delta t}{2\mu_x(i,j,k) + \Delta t\sigma_x^m(i,j,k)} \tag{24d}$$

In Figure 5, E_{x} value is updated with update equation 21. H_{z} and H_{y} terms are visualized at the figure.

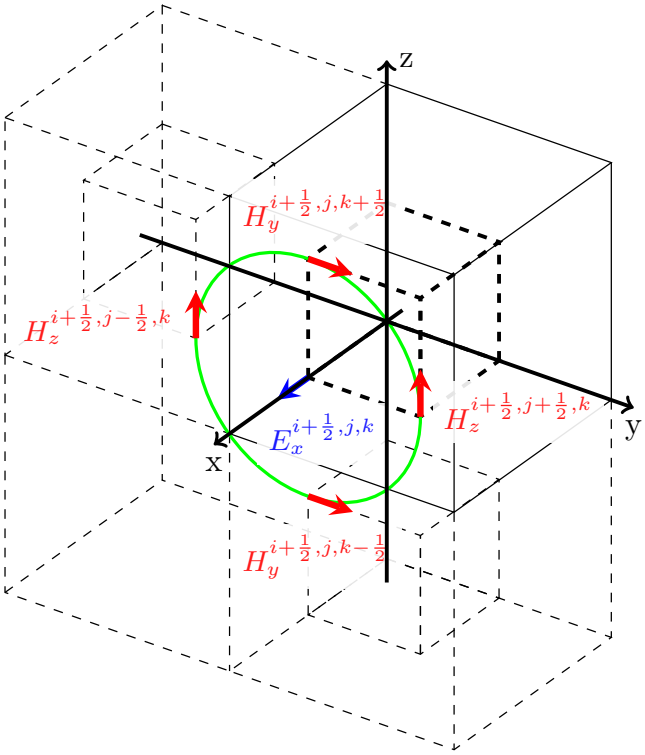

Figure 5. Updating E_{x} value from adjacent H_{z} and H_{y} field values

In appendix 2 all six update equations are defined. These six update equations are only required in 3D FDTD simulation.

4.1.1 Perfectly Matched Layer (PML)

Due to the memory limitations of computers, it is necessary to limit the size of the simulation to only relevant area. Simulation area and infinity need an interface where waves from simulation can pass through to the infinity. Perfectly matched layers (PML) are solution to this problem. In PML waves are slowly absorbed into perfectly matched layer with minimal reflection back to the simulation area.

In 1994 Jean-Pierre Berenger published article where he formed first PML using Maxwell's equations [21]. In the article, he presents new impedance matched absorption layer that does not reflect radio waves. In the simulation area and in the PML area impedance are matched which prevent reflection with every incident angle and frequencies [17].

PML is located on the edge of the simulation, where it interfaces with the infinity. In PML

losses are implemented slowly using fictitious conductivities, PML act as anisotropic medium. [17]

5 SIMULATION

In this chapter, the simulation environment is examined. The chapter introduces how simulation is designed and implemented in this thesis. The purpose of the simulation environment is to include all the necessary tools from the simulation of radio waves to the analysis of the simulation results. The simulation environment is implemented in the Matlab programming language, but some tools uses other programming languages, such as Python.

5.1 The office modeling

The simulation environment requires some kind of model of the test environment that can be used to illustrate the attenuation of the wave by the materials. The easiest way to model a test environment is to do the modeling with a CAD (Computer-aided design) program. CAD software can be used to position walls using floor plans, and it is also easier to scale the model for match reality. Unlike coordinate-based modeling, CAD software can set the relative distances between walls, and wall modeling provides a visual representation of structures.

5.1.1 Model scaling

A colored 2D sectional image is taken from the model and the image is imported into the simulation. In the simulation, the sectional image has to be scaled to corresponding resolution and the actual scale of the environment. Using the section image is the easiest way to bring the models into the simulation. Also the resolution of the section image must be large enough not to affect the accuracy of the simulation. The best way to import models would be to make a library that would change the shapes into code and set the parameters in the code for the materials. This method was not used in this thesis because it would have taken too much time to make the library and accuracy of the sectional model is good enough not to have an effect on the simulation outcome.

The sectional image requires processing before it can be imported into the simulation, the image must be scaled to match the resolution set in the simulation and the actual scale. The resolution of the section image must be equal to or greater than that of the simulation. If the resolution of the simulation is higher than the sectional image, the

separation different materials and wall shapes in the simulation is impaired. Importing too thin materials for simulation is impossible.

If the resolution of the sectional image is greater than that of the simulation, the scaling can better take into account thin materials that are narrower then the simulation resolution (one tenth of the wavelength). In scaling, 2 by 2 squares are averaged into one value, in which case the values of thin materials can be taken into account. This scaling affects the surface reflection of the materials, but the effect is not significant in comparison with not detecting thin materials like glass or metals.

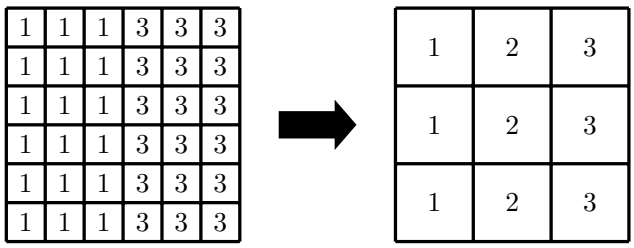

Figure 6. Example of two material interface scaling.

In figures 7 and 8 differences between reflectance and transmittance are examined at example the interface presented in Figure 6, where the waves are moving from left to right. It can be seen from the figures that scaling causes little changes in reflectance and transmittance, the changes are not significant compared benefits of scaling.

The reflectance and transmittance shown in Figure 7 are parallel to the plane of incidence. In the scaled case, waves are transmitted more to the material.

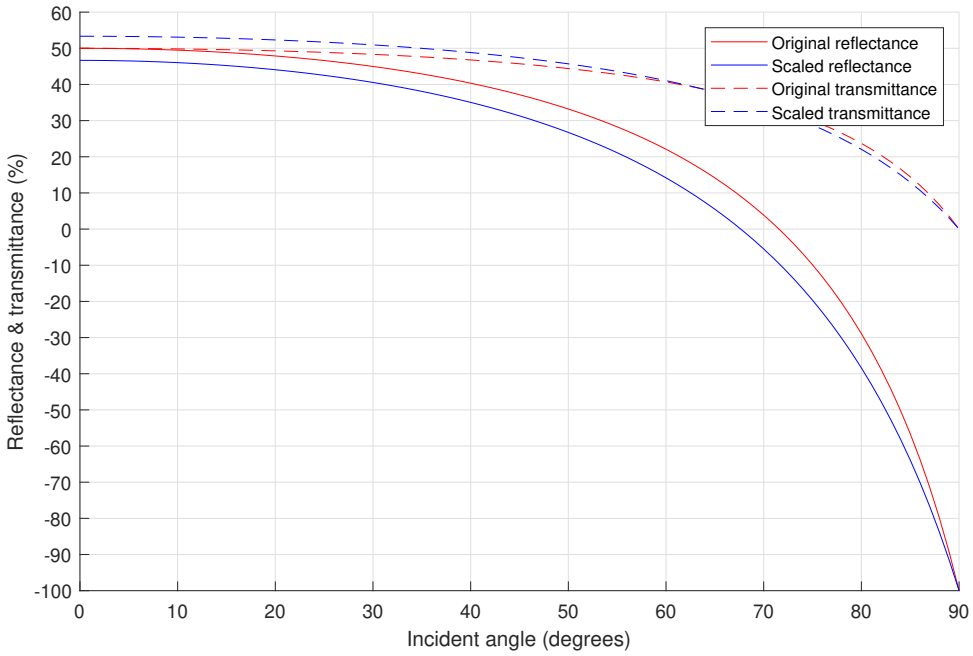

Figure 7. Orginal and scaled interface reflectance and transmittance parallel to the plane of incidence.

The reflectance and transmittance shown in Figure 8 are perpendicular to the plane of incidence. As in Figure 7, waves are also transmitted more to the material.

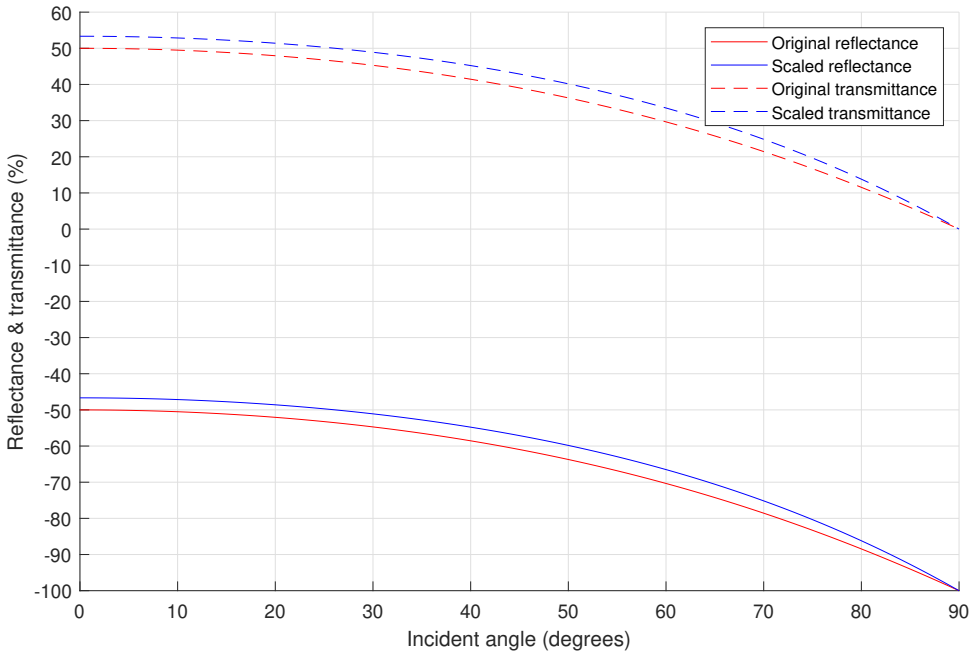

Figure 8. Orginal and scaled interface reflectance and transmittance perpendicular to the plane of incidence.

The transmittance increase can be explained by the angle of incidence of the first and second layer of material. As the wave enters the material from the air, the angle of refraction refracted more than in the scaled case where waves are refracted gradually. Due to the gentler angle of incidence, the waves are transmitted more to the material.

5.2 FDTD simulation

The simulation is based on the theory discussed in the previous chapter. At the beginning of the simulation, the variables required for the simulation are calculated or defined. At the same time, the office model is processed and the values of the materials are assigned to the material map. In the material map, the locations of the walls and objects are stored and the parameters of the materials are defined.

After initialization, the simulation can be started. In the main loop of the simulation, the values of the electric and magnetic fields are updated based on the previous and adjacent values. The simulation is continued until the desired iteration is reached. Usually, simulation is run until reached steady-state where simulation doesn't change or changes

are insignificant after a curtain time. In this thesis, steady-state was reached after 30 000 iterations. Flowchart of the simulation is shown in appendix 1.

5.2.1 Basic update function

The simulation was implemented in two dimensions because the heights of the rooms are not easily readable from the floor plans. The disadvantage of two-dimensional simulation is the height differences, the transmitting (TX) and receiving (RX) devices must be at the same level in the testing in order for the measurements to correspond the simulation.

The advantage of a two-dimensional simulation is the speed of the calculations, a two-dimensional simulation requires the calculation of three values at the measurement points (TM: Ez, Hy, Hx, TE: Hz, Ey, Ex). In a three-dimensional simulation, the calculations of all six values are required.

Appendix 3 shows the required upgrade equations for the TM and TE modes.

5.2.2 Simulation resolution and sampling

The resolution of the Yee grid is affected by the wavelength of the source used, in order to simulate the propagation of the waves in the simulation, the grid density must be less than the source wavelength. In general, 10-20 measurement points per wavelength are usually required [20]. At 2.4 GHz, the wavelength is about 12.5 centimeters, giving a grid resolution (Δx, Δy and Δz) between 0.625 and 1.25 centimeters.

The time between updates must be small enough for the simulation to be stable. When waves move in three-dimensional space, the distance traveled must correspond the time required to move from point A to point B in reality. In a free space, the propagation speed of waves is the speed of light, after the simulation has progressed by one unit of time in three-dimensional space, the distance from the starting point must be the same as the propagation of light at the same time. The time difference required for simulation stability can be calculated using the Courant–Friedrichs–Lewy condition (CFL condition) [17].

$$\Delta t \leq \frac{1}{c\sqrt{\frac{1}{(\Delta x)^2} + \frac{1}{(\Delta y)^2} + \frac{1}{(\Delta z)^2}}} \tag{25}$$

Where c is the speed of light and Δ values are the grid resolution on x-, y- and z-axis.

The grid used in this thesis is in two-dimensional space, then the value of Δz is zero. From equation (25) the term Δz can be ignored.

The CFL value indicates the largest possible time difference between updates, in this thesis a CFL value of 0.99 time has been used in order to make the radio waves propagate as realistically as possible in the simulations, however, while keeping the simulation stable.

5.2.3 Simulation dimensions

In addition to the grid resolution, also the actual dimensions of the office model determine final size of the simulation. Depending on the situation, by changing the grid resolution, the size of the simulation can be increased or decreased to match the desired size. In large simulated areas, the resolution should be kept low and in simulations that require more accuracy, for example in the simulation of edges and angles, it is worth increasing the resolution. In two-dimensional simulations, as the X- and Y-axis points doubles, the number of points calculated in the simulation quadruples.

In the simulated office model, the grid resolution was 1.25 centimeters (frequency 2.4 GHz and the resolution on the x and y axes are equal) and the actual size of the model was 43.50x20 meters. Based on these values, the size of the simulation became 3482x1601 measurement points. At the edge of the simulated areas, there is a 20-point-thick UPML (Uniaxial Perfectly Matched Layer) area where four values are calculated for each point (Hx, Hy, Ezx, and Ezy) and within the simulated area, three values are calculated for each point (Hx, Hy, and Ez).

The size of the simulation must also take into account the amount of RAM (random access memory) required, Matlab allocates 64 bits (8 Byte) of memory for each cell array item. In small simulation areas, the amount of memory is not significant, for example, a 1000x1000-simulation area requires 8MB (Megabyte) of RAM. It should also be noted that there are three cell arrays for each measurement point.

In the simulated office, 45MB of RAM is required for each cell array. The resolution of the simulation could be increased, but it would take more time and processing power to update larger arrays.

5.2.4 Time domain to frequency domain

Analyzing the results from the simulation can be difficult in some cases, especially over short or long time periods. The values obtained from the simulation can be converted into the frequency domain for easier frequency analysis. In the frequency domain different frequencies can be isolated from each other.

When time between measurements (Δt) is known, the measured values can be transformed to the frequency domain, using Fourier transform formula. In equation 26 sampled array is transformed from time domain to the frequency domain.

$$X(\omega) = \Delta t \sum_{n=1}^{n=N_{\text{step}}} x(n\Delta t)e^{-j\omega n\Delta t} \tag{26}$$

where ω is angular velocity of source, N_{step} is current time step and x is sampled array.

5.2.5 Output

Any variable can be selected as output, for this thesis electric field array is used as an output of the simulation. In this thesis vertically polarized waves are used in testing, it is important to determine the value of the electric field to determine the attenuation of the wave and the strength of the signal. The electric field can be used to measure the values of the electric field from certain points and to visualize the attenuation of the electric field under the influence of materials and distances.

To make the electric field values easier to understand, the electric field must be changed from the time domain to the frequency domain, using equation 26. At the frequency domain, 2.4 GHz waves can be isolated, giving the wave amplitude at a certain point. In Figure 9 path loss is plotted, in the figure attenuation and reflections from materials are visualized. In the figure, the simulated transmitter was placed at measurement point 3 (X 7m, Y 14m), transmitter point was used as the reference value in the decibel scale (at the transmitter point path loss was 0 dB).

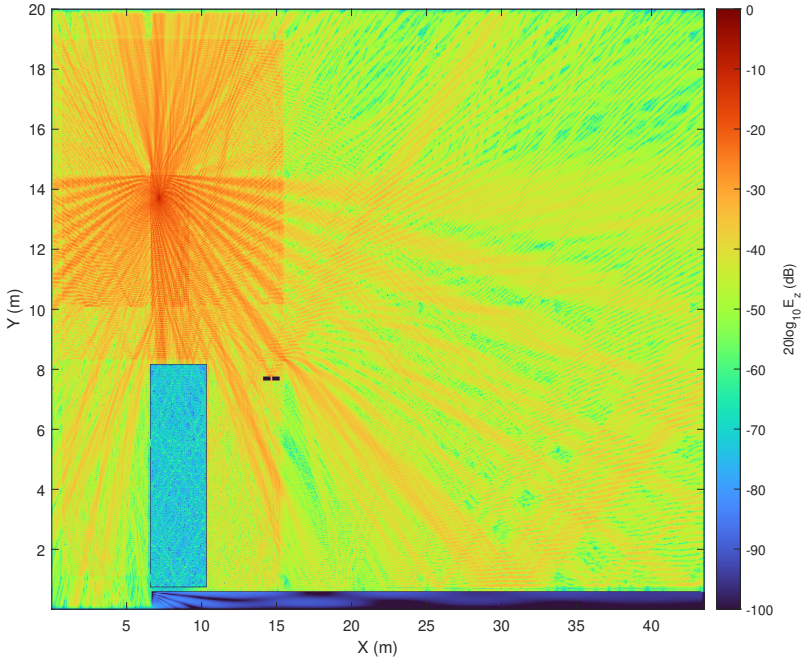

Figure 9. Path loss in a decibel scale, the simulated transmitter is located at measurement point 3.

6 MODELING AND MEASURING OFFICE ENVIRONMENT

In this chapter, the office model and measurements are examined. The modeling section reviews the things that were taken into account from the modeling of the office to the materials used in the structures and how the modeling took place. The measuring section reviews the operation of the test equipment and how the testing was performed in the office.

6.1 The office model

In office modeling, old floor plans was used in modeling. From the floor plan, the layout of the wall can be obtained. Various changes to the layout had been made over the years, these changes cause slight differences between the building and the floor plan.

6.1.1 Building materials

In Finnish buildings, the wall structures are relatively simple. The exterior walls have exterior cladding and rainscreen, windliner, insulation, load-bearing structure, vapor control layer and interior cladding [22]. For exterior cladding materials such as wood, profiled sheet metal, brick or concrete can be used. For Load-bearing structure usually used reinforced concrete or wood. In the office modeling, the windliner and vapor control layer were ignored because the resolution of the simulation is not accurate enough to model the vapor control layer and the windliner was completely omitted from some of the exterior walls.

The interior walls have interior cladding on both sides, load-bearing structure and insulation (sound proofing) in the middle [23]. The most common material for interior cladding is gypsum board, but in the office, some of the rooms used fiber-based material for interior cladding. In interior walls, load-bearing structure is usually made of wood. The insulation of the external walls varied depending of construction year, the most common insulation in the office was glass and mineral wool. In the simulation, it was assumed that all insulators are glass wool.

The load-bearing structures are generally cast in concrete or brick, both load-bearing

structures were used in the office. The building had concrete support pillars at certain distances each other and one almost uniform brick wall.

The properties of the materials used in the simulation, such as permittivity and permeability, have been collected from several different sources, the values vary little between different sources.

6.1.2 Modeling

The office model was modeled with CAD software (Autodesk Fusion 360). The floor plan was imported into the program as a background on where walls and objects were modeled. The model was modeled in two-dimensions but three-dimensions modeling is also possible. In this thesis two-dimension model was chosen due to thesis subject defining. The modeling takes into account materials at a height of one meter from the floor surface, such as windows.

The wall thicknesses or materials are not marked into the floor plan, in the model wall thickness and material were assumed to be the same in all interior walls. In some walls were fire insulation (metal layer), which was modeled separately.

In the model, the materials are color-coded with their own colors, which means that they can be easily imported into the simulation.

In Figure 10, the office model used in the simulation is shown. In the figure, load-bearing materials reinforced concrete and bricks are colored yellow and orange, respectively. Insulation and sound proofing is colored green, interior cladding is colored blue, wood is colored brown and glass is colored aqua.

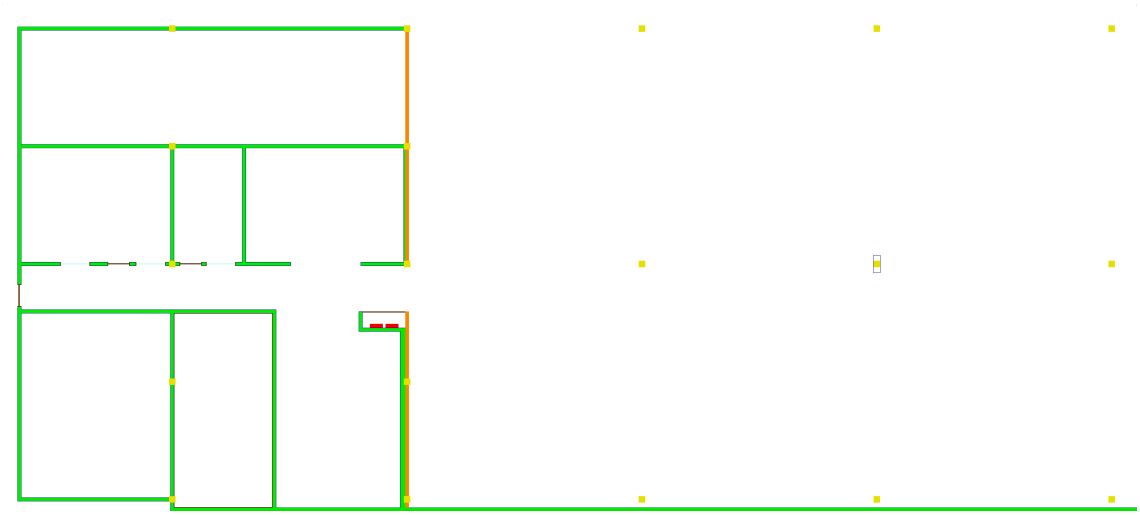

Figure 10. The office model

6.2 Measurements

In order to be able to analyze the results obtained from the simulation, a measurement must be performed in the office from which the simulation model is made. When making measurements, things that may affect the results of the measurements, such as reflections, must be taken into account.

6.2.1 Testing equipment

In testing Bluetooth development kit (Nordic Semiconductor NRF52840 DK) was used. Bluetooth development kit was chosen because Bluetooth devices had become more common in office environments and development kits are widely available. Testing requires at least two development kits, a signal transmitting (TX) and a receiving (RX) devices.

The testing program was developed where the transmitting device continuously transmits advertising packets and the receiving device reads only the signals of the predetermined device. In the testing transmitting power of the transmitting device was set to 1 milliwatts or 0 dBm (decibel-milliwatts). The real transmitting power was not measured but it is assumed to be close to the set value. A serial connection is established to the receiving device, the receiving output prints the received signal strength indication (RSSI) values, and 50 values are printed per measuring cycle. Several values are stored during the cycle in order to reduce the interference caused by reflections.

A unique identifier number is created for each measuring cycle, the identifier number ensure that measurements are not confused with each other. Identifier numbers are stored in the measurement report where values can be imported to analysis script. Identifier numbers are also stored in the same log file as signal strength measurements. In analysis identifier numbers are read from measurement report and identifier numbers are matched with signal strength measurements from log file.

The devices do not establish a connection with each other also known as pairing. The transmitting device only sends advertising packets and receiving device measures received packets strength (RSSI). The connection between devices is not required to measure signal strength, the receiving device only requires to receive advertising packet. To receive the package the receiving device must be sensitive enough to detect signal, Bluetooth development kit used in testing have the sensitivity of -96 dBm.

6.2.2 Measurment points

The measurement points were chosen to test the office layout as diverse as possible. The placement of the measurement points took into account the different materials of the walls, the angles between the walls and the wave, and the different distances from the transmitting device.

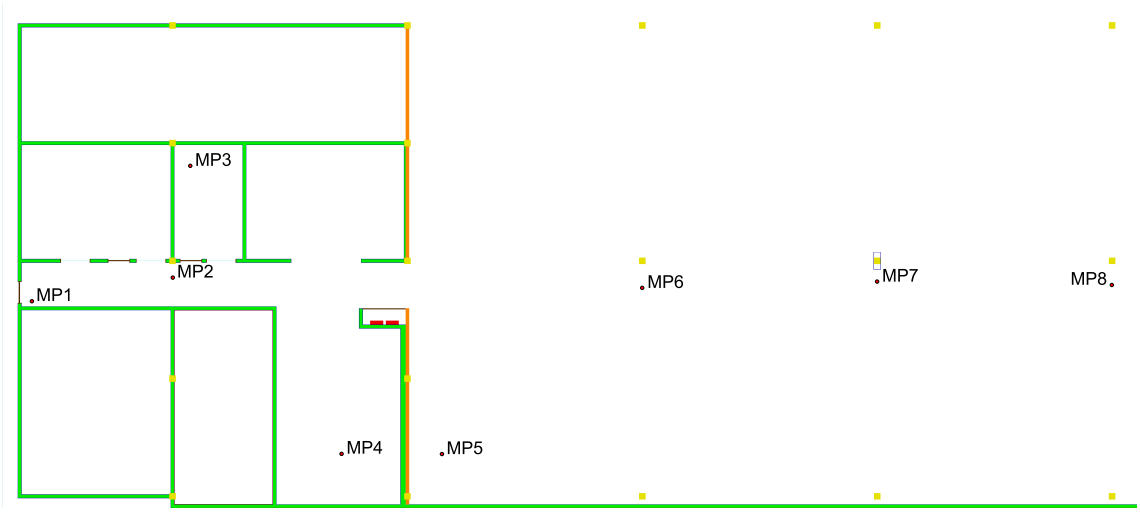

Figure 11. Measurement points in the office model

The test equipment was placed one meter above the floor so that antennas of the trans-

mitting and the receiving devices were at the same height. The distance between the measurement points and the walls was more than 50 centimeters, this allows the receiver to be moved closer to the wall when measuring multiple measuring cycles.

At the measurement point multiple measuring cycles are measured to make sure that interference does not have an effect on measuring. After measuring cycle the receiving device is moved a little bit from the measurement point, first north-south direction then west-east direction from the original point. This movements reduce constructive and destructive interference cause by reflecting waves. In measurements, the receiving device is moved about 6.2 centimeter which is half wavelength of 2.4 GHz wave.

7 RESULTS AND DISCUSSION

The performance of the simulation was analyzed by taking eight measurement points (shown in Figure 11), two results are reviewed in this chapter. In this chapter measurement points 1 and 6 are examined. The measurement points to be reviewed are chosen because they offer the widest possible and different scenarios in relation to each other.

Measurement point 1 was chosen because the measurement point can be used to simulate the effect of distance on the signal and there is a lot of material between the measurement points. The second measurement point, measurement point 6, was chosen because it differs significantly from 1 measurement point. There are not many walls near the measuring point, so it is possible to observe how the waves propagate in free space.

7.1 Simulation

The simulation used the theory and the simulation environment presented in the previous sections. In both measurement points, independent simulation environment instances were used, i.e. the simulations do not affect each other. In the simulation, a sinusoidal source with a frequency of 2.4 GHz was placed at measurement point, the amplitude of the wave does not affect the final result of the simulation.

In the simulation, at each iteration, the electric field array was transformed to a frequency domain and the frequency domain value was summed to the previous value. The frequency domain array can be used to determine the peak value of the electric field at a certain point and at the same time find out the attenuation of the wave.

A simplified model of the office was used in the simulation. The furniture has not been taken into account in the modeling, only the walls have been modeled in the simulation. The locations of the walls remain in the same location in the office at all times, except for interior walls, the placement of which may change over time, but in general the walls remain in the same location throughout the lifetime of the building. Furniture layouts and fixtures can change several times during the lifetime, so accurate modeling of the furniture doesn't make sense.

The simulation was run until reached 30,000 iterations, after that no major changes occurred in the simulation. At that point, the simulation reached steady-state.

In figures 12 and 14, are shown the results obtained from the simulations. The values of the results are obtained from the frequency domain array and the values are collected from the same points as the measurement points are placed in Figure 11. The values in the figures are the average of values around the measurement point in radius of two points. Point average is used because of "hot" and "cold" spot caused by reflection interference. Averaging values round the measurement point prevents these hot and cold spots. These hot and cold spot are also in the office measurements, where the effect is prevented by moving the measuring equipment little bit sideways.

In Figure 12, the sinusoidal source was positioned in measurement point 1. The values in the figure are the attenuation values between the transmitter point and the measurement points. The values are given in a decibel scale. The values seem to be relatively logical excluding a few exceptions. In measurement points two to five values are increasing with distance, but in points six to eight, the values do not increase with distance. In points 6-8 values should grow steadily because the distance between the points is the same and there are no materials between the points. The differences between the points can be explained by reflections, either destructive interference occurs at 6 points or constructive interference occurs at 7 and 8 points.

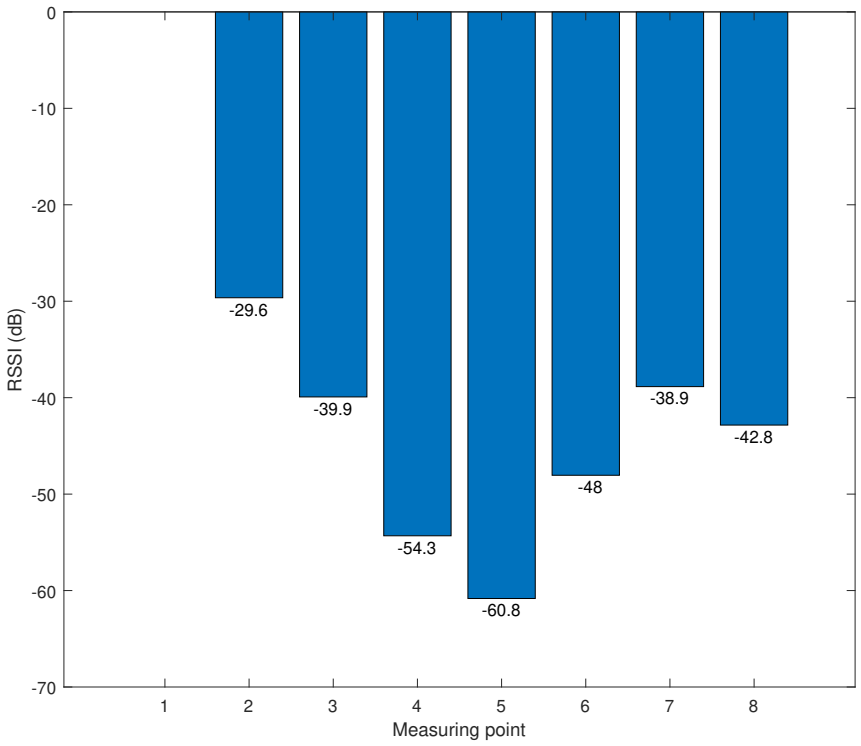

Figure 12. Attenuation values, sinusoidal source positioned at measurement point 1.

In Figure 13, the measurement points are marked with black crosses. It can be seen from the figure that destructive interference occurs at measurement point 6 and constructive interference may occur at measurement points 7 and 8.

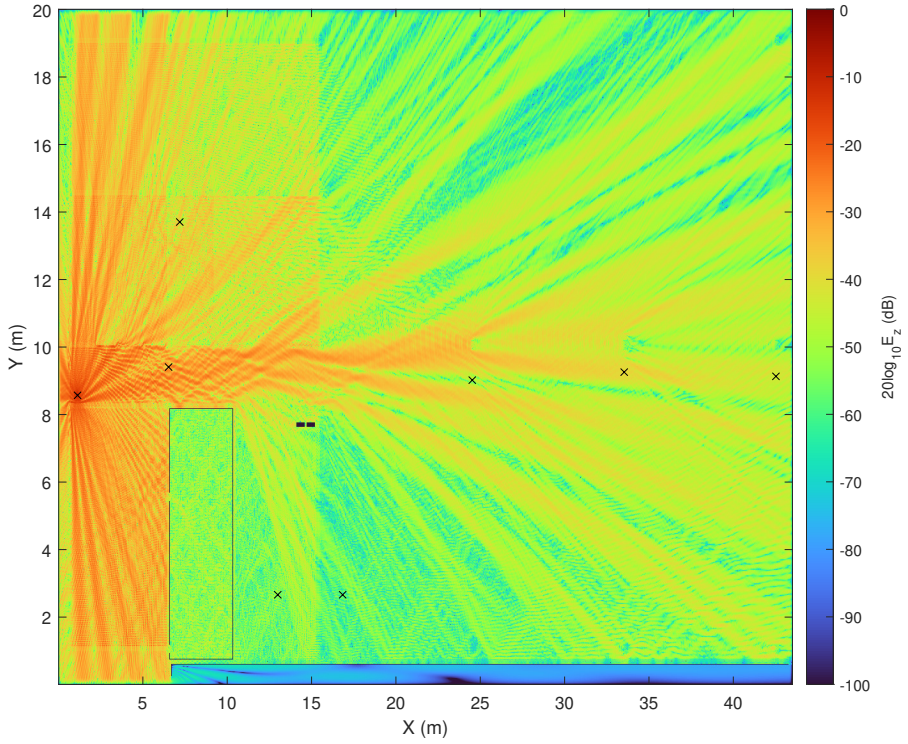

Figure 13. Path loss in a decibel scale, the simulated transmitter is located at measurement point 1.

In Figure 14, sinusoidal source positioned in measurement point 6. Measurement points 5 to 7 have a direct line of sight to the source, measurement points 5 and 7 have the most same distance to the source and when distance increase the value also increase as in the measurement point 8. The differences between the values may be too small. There is a brick wall between the transmitter and measurement points 3 and 4 that attenuates the wave. There is also an interior wall between the measurement point 3 and the brick wall, which in turn dampens the wave further, hence the difference between the measuring points 3 and 4. The value of measurement point 1 is too high if you compare with the value of measurement point 2. Both measurement points have a direct line of sight to the transmitter, in which case the value of measurement point 1 should be slightly higher than those of measurement point 2 due to the distance.

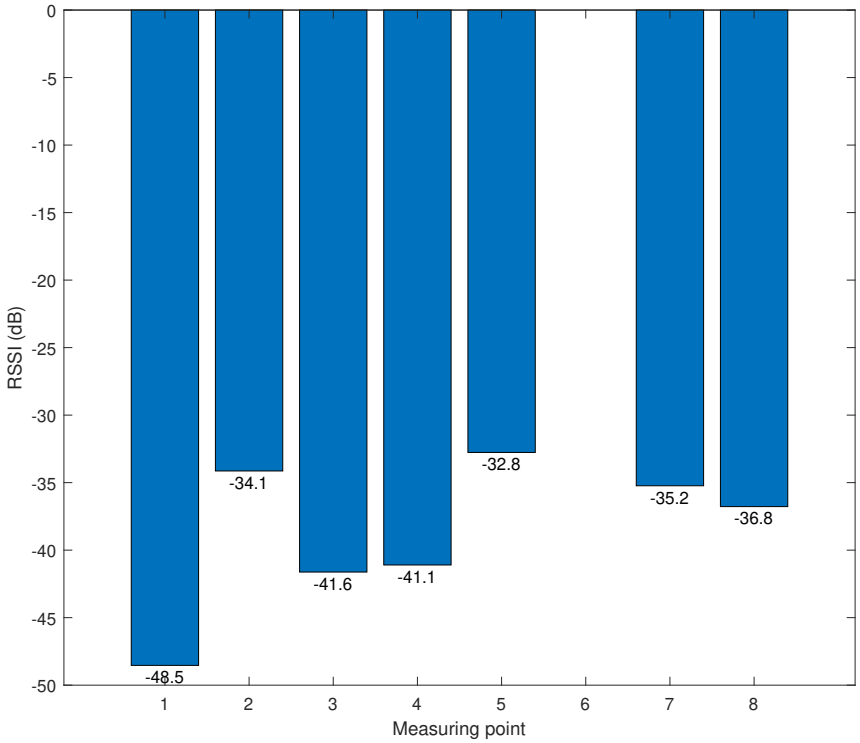

Figure 14. Attenuation values, sinusoidal source positioned at measurement point 6.

In Figure 15, the measurement points are marked with black crosses. It can be seen from the figure that there is a lot of destructive interference due to the wall at the measuring point 1, due to this the value is much higher than expected. It can also be seen from the figure how radio waves are spreading in simulation area evenly, due to the absence of nearby walls.

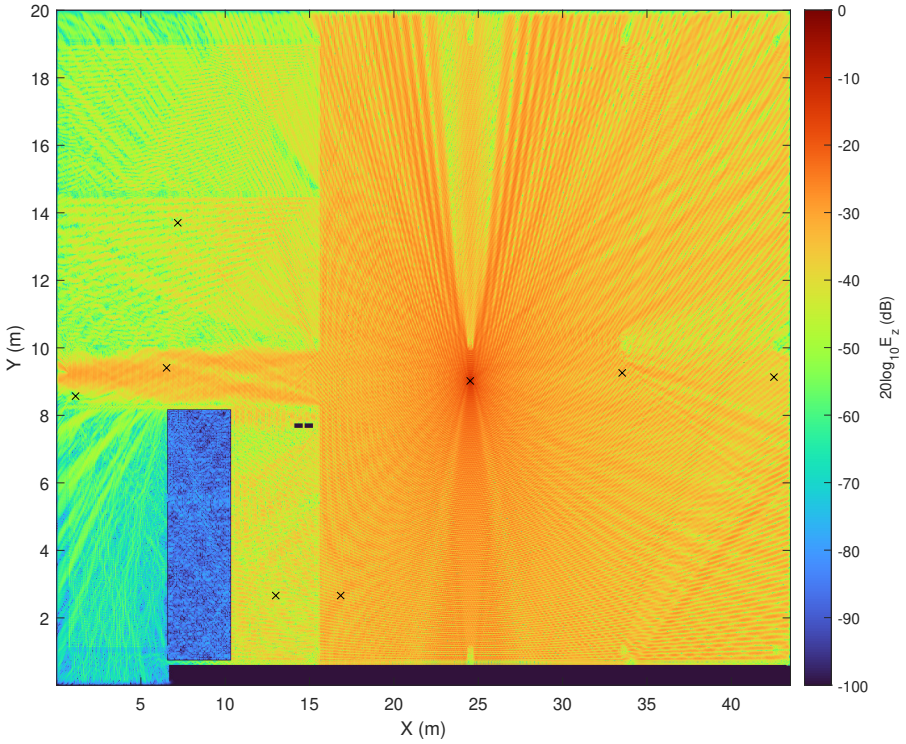

Figure 15. Path loss in a decibel scale, the simulated transmitter is located at measurement point 6.

7.2 Measurements

The measurements were performed in a furnished office, the effect of the furniture has not been taken into account in the simulation. The largest pieces of furniture have used a wood frame and fabric for upholstery, and some pieces of furniture have also used metal parts that significantly affect the propagation of signals.

In the measurements, the position of the transmitter was set to a certain point, after which all the other measurement points were measured one at a time. Five measurement cycles were taken at each measurement point, which can be used to average the obtained measurement values. By averaging, the interference caused by the reflections can be reduced.

The identifier number obtained from the measurement point was recorded in the measurement report, from which it is read in the analysis phase. 50 measurements (RSSI values) are taken from the measurement points, in the analysis phase the most common RSSI value is taken from those values. The most common RSSI value can be determined with

the help of the mode, when the measurement data is enough, the effect of noise is reduced.

In Figure 16, the transmitter was place at measurement point 1. Measurements were performed in sequence at all other points, at each point five measurement cycles were performed to reduce reflections. In the figure, the RSSI values are the average of five measurement cycle modes.

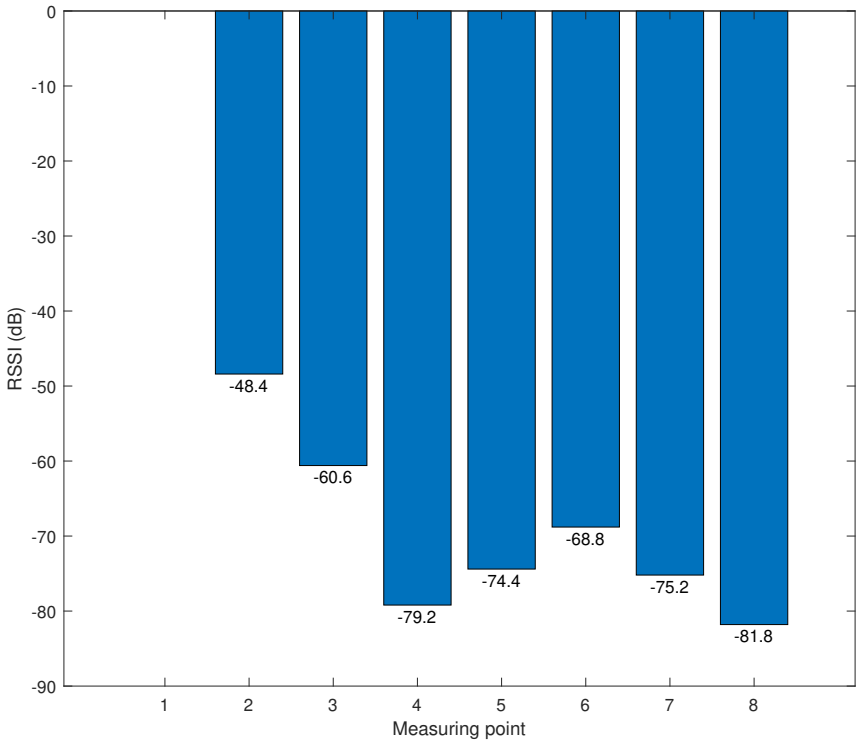

Figure 16. The transmitter positioned at measurement point 1.

In Figure 17, the transmitter was place at measurement point 6. The RSSI values are the average of five measurement cycle modes.

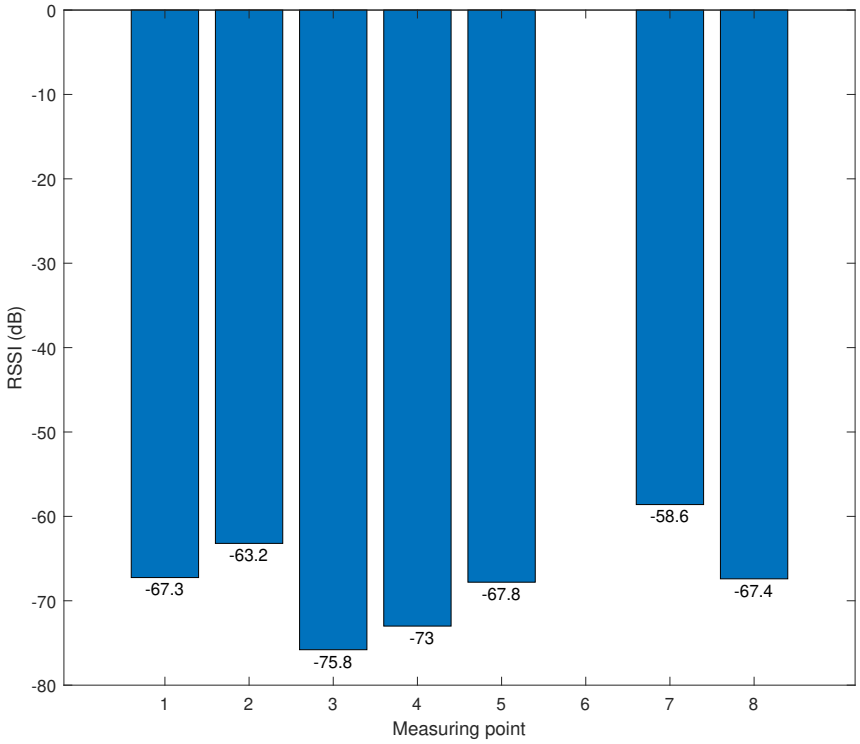

Figure 17. Transmitter positioned at measurement point 6.

7.3 Analysis

The measurement results are analyzed by comparing the simulated and measured values from the same points. All comparable values are presented in the previous paragraphs.

The results of the simulation and measurement shown in Figures 18 and 19 when the transmitter is placed at measurement point 1. In Figure 18, the raw values obtained from the simulation and the measurement are shown in the same figure without modification. The values of both are presented on a decibel scale. In both figures the measured values are in blue and the values simulated are in orange. The simulated and the measured values are shown below the rectangles.

The same values are shown in Figure 19, but an offset equal to the smallest difference between the simulated and measured values is inserted in the simulated values (in this case difference in measurement point 2). Setting the offset makes it easier to highlight the differences between measurements. In Figure 19, the difference between the simulated

and measured values is shown below the rectangles.

In Figure 18, there are significant differences between the simulation and the measurements, as noted in the simulation points from 6 to 8, the waves should attenuate as the distance increases. This attenuation can be observed in the measurement. At points 4 and 5, the values are wrong way round in the simulation, this may be due to the brick wall between points 4 and 5. In the simulation, the properties of the wall materials may not correspond to the actual values, then the wall reflects the waves better than conducts. There may also be some unknown material between the brick wall and the surface materials that has not been taken into account in the simulation.

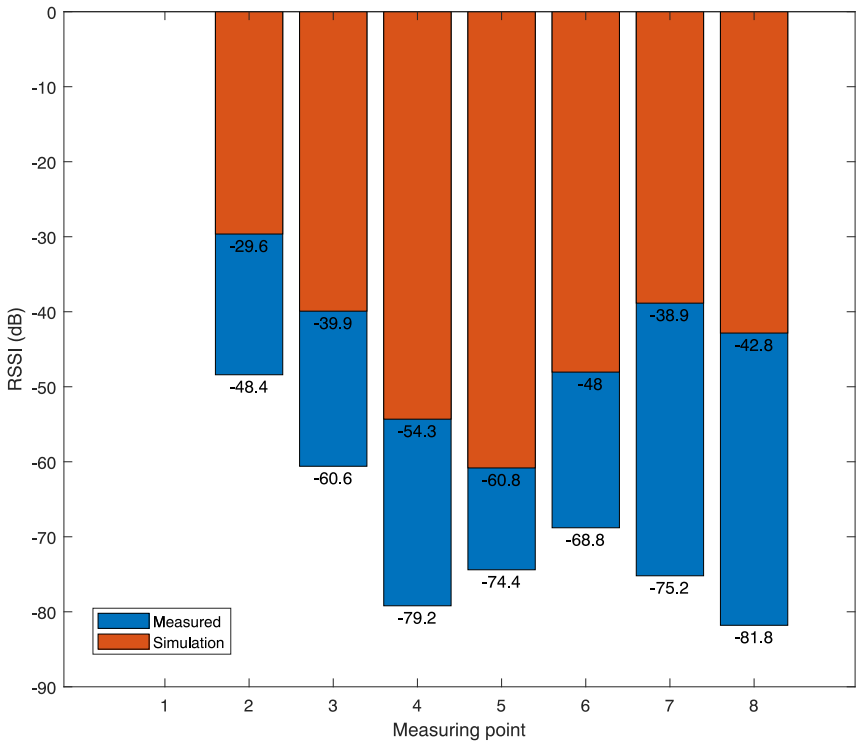

Figure 18. Measurements versus simulation. The transmitter positioned at measurement point 1.

In Figure 19, it can be seen that the measured values are higher than the simulated values, except at measurement points 7 and 8. At measurement points 7 and 8, it can be seen that constructive interference may occur in the simulation because the difference is negative at measurement point 6.

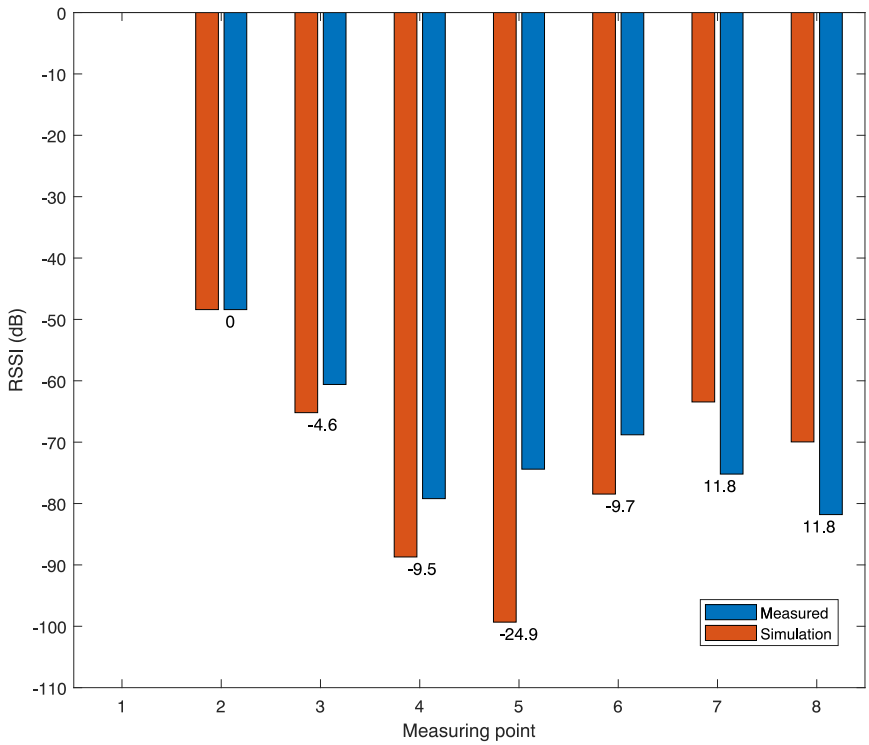

Figure 19. Simulation offset according measurement point 2 (nearest point). Transmitter positioned at measurement point 1.

The simulated and measured values of measurement point 6 are shown in figures 20 and 21. In the same way as in the measurement point 1, the raw measured point values are shown in Figure 20 and an offset has been added to the simulated values in Figure 21, which is the difference between the simulated and measured value of the nearest measurement point (measurement point 7). In both figures, the simulated values are in orange and the measured values are in blue.

It can be seen in Figure 20 that the differences between the values of the simulation and the measurements are high, but the differences between the points are similar. The differences between the values of measurement points 3 and 4 are smaller in the simulation and the value of measurement point 5 is smaller than it should be.

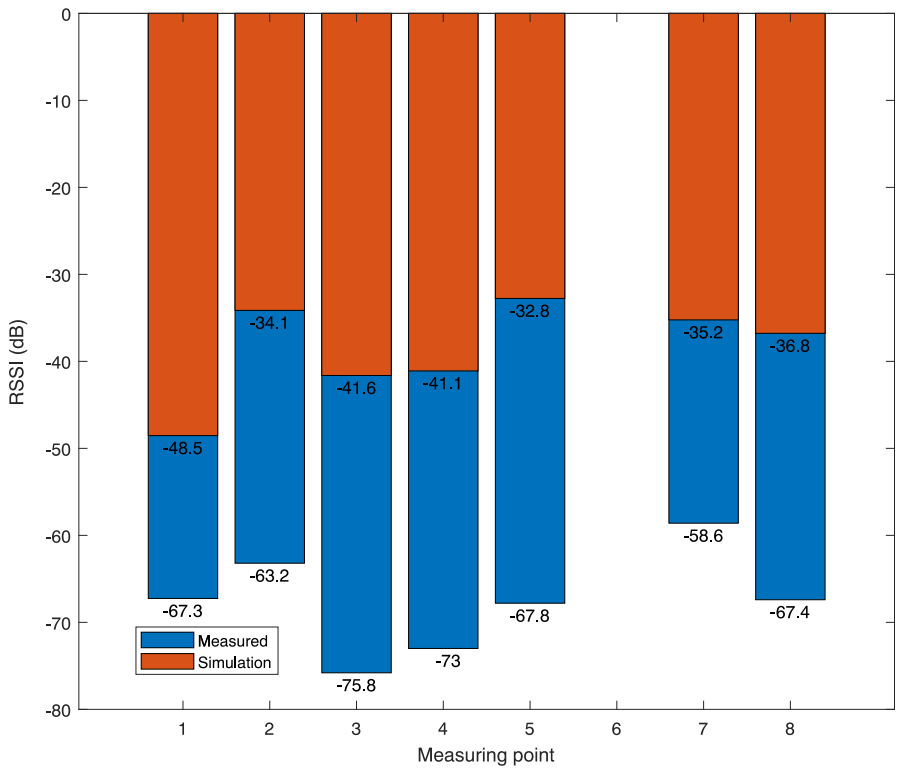

Figure 20. Measurements versus simulation. Transmitter positioned at measurement point 6.

In Figure 21 it can be seen that the measured values are higher than in the simulation, in the case of measurement point 1 the values were the other way around. At measurement points 1 and 5 the differences in values are the largest, at other points the difference in values is less than 10 decibels. The attenuated signal obtained in the simulation of the measurement point 1 is due to the wall reflection, Figure 15 shows how in the simulation destructive interference is formed at the measurement point from the wall reflections. The weaker result obtained in the measurement point 5 is difficult to explain.

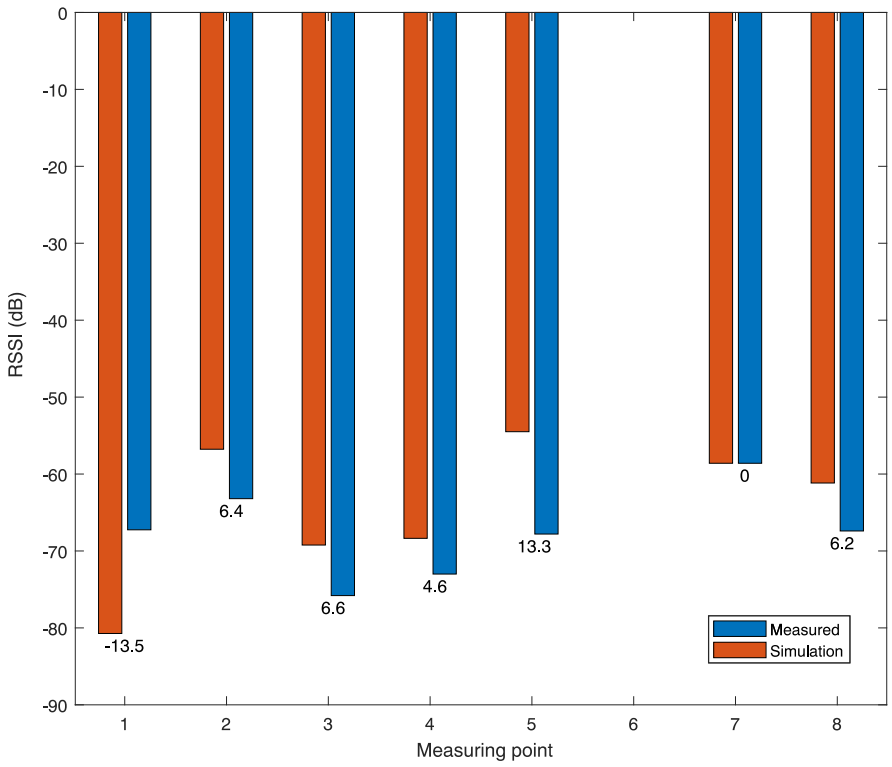

Figure 21. Simulation offset according measurement point 7 (nearest point). Transmitter positioned at measurement point 6.

7.4 Results

The differences between the values obtained from the measurement and the simulation are high if the values are raw. The values obtained from the simulation are much higher than the values of the measurement. The difference in values can be affected by the transmission power of the device used in the measurement, set transmitting power (1mW) is the power before the antenna. In the antenna, the value of the transmission power decreases due to antenna losses. In reality, the power transmitted by the antenna is less than 1 mW, which could explain the lower values of the measurements. The effect of the antenna radiation pattern on the measurements was also not taken into account in the testing. In order for the radiation pattern to be taken into account in the simulation, antenna modeling would be required. The resolution of the simulation is too high to model the antenna.

When an offset corresponding to the difference in measurements is applied to the simulation results, the results begin to become valid for comparison. The differences obtained in

the simulation and measurement are relatively small, but in some cases the values throw significantly apart.

The differences in the results may be due to the materials used in the simulation, the values used in the simulation have been obtained from the Internet and the values are common to certain materials. The materials used in Finland may differ significantly from the values of materials used in Central Europe, for example. Improving the simulation would require measuring each material or determining the values of the reflection and refractive indices of the walls, measuring the materials would take a lot of time, and the results obtained from the simulation may still differ in reality.

The simulation presented in this thesis gives indicative values, the values obtained from the simulation can be scaled to correspond to the measured values, but scaling is laborious and to some extent unnecessary work. From the path loss figures (13 and 15) obtained from the simulation can give an idea how the radio waves move in the office space. With path loss figure transmitters and receivers can be placed in the office, this approach still requires testing to get the best possible connection between the devices.

7.5 Future work

A further study would be how much the simulation could be improved by modeling the office more accurately and how accurately the model should be modeled before the time spent on the simulation exceeds the benefits of the simulation.

Another object of further research is the simplification of wall structures, is it possible to justify the modeling of the wall with the values of reflections and refraction? The refractive and reflection coefficients of the wall would be measured, and based on these values, a wall of homogeneous material would be created. In this way, wall modeling would be speed up and possibly wall models would be more realistic.

Last object of further research is the implementing antenna radiation pattern into simulation. Is it possible to put a certain radial attenuated material around the transmitter that attenuates radio waves the same way as the radiation pattern? This attenuating material should be impedance matched with an empty simulation environment so that the material does not cause reflections and the attenuation of radio waves in a particular direction can be modeled using the conductivity of the material. In this way, the problem would be the radius of the material, in order to accurately model the radiation pattern, the radius of the

material is required to be large and the value of the reflected waves passing through the material is affected by the large radial material.

8 CONCLUSION

In this master's thesis, radio wave simulator was designed, developed and tested. The purpose of the simulation is to create an illustrative figure of the propagation of radio waves in the office environment.

The basic of radio waves and the behavior of radio waves were discussed. The behavior of radio waves depends on the properties of the materials, based on these properties, the propagation and reflection of radio waves in the material and at the same time in the office environment can be simulated.

The office environment modeling and finite-difference time-domain were discussed. The office can be modeled using the floor plans of the office and the materials can be brought into the simulation using the model. Importing the model into the simulation is successful, without any problems. In the simulation, the electric and magnetic fields can be updated using the equations shown in Appendix 3. The simulation is stable when the time difference and resolutions are set below the CFL-value and a tenth of the wavelength, respectively.

Based on the simulation and measurement results, the simulation values do not match the measurement values. The values require processing, after which the values are comparable with respect to each other. The values obtained from the simulation are indicative, which can give an idea of the possible behavior of radio waves in office environment.

REFERENCES

[1] David J. Griffiths. *Introduction to Electrodynamics*. Cambridge University Press, 4 edition, 2017.

[2] Philip Ronan. *EM spectrum*, 2007. [Online; accessed Nov, 26, 2020]. Retrieved and adapted from: `https://commons.wikimedia.org/wiki/File:EM_spectrum.svg` under the CC BY-SA 3.0 license.

[3] International Telecommunication Union. *Nomenclature of the frequency and wavelengh bandsused in telecommunications*. https://www.itu.int/rec/R-REC-V.431/en, 08 2015. Recommendation ITU-R V.431-8.

[4] IEEE Aerospace and Electronic Systems Society. *IEEE Standard Letter Designations for Radar-Frequency Bands*. *IEEE Std 521-2019 (Revision of IEEE Std 521-2002)*, pages 1–15, 2020.

[5] Finnish Transport and Communication Agency. *Radio frequency regulation*, 04 2020. Regulation 4Z/2020M.

[6] International Telecommunication Union. *Radio Regulations Articles Edition of 2020*. https://www.itu.int/pub/R-REG-RR-2020, 2020.

[7] Massimo Mitolo and Rodolfo Araneo. *A Brief History of Maxwell's Equations [History]*. *IEEE industry applications magazine*, 25(3):8–13, 2019.

[8] James Clerk Maxwell. *A dynamical theory of the electromagnetic field . Philosophical Transactions of the Royal Society of London*, 155:459–512, 1865.

[9] D. L. Sengupta and T. K. Sarkar. *Maxwell, Hertz, the Maxwellians, and the early history of electromagnetic waves*. *IEEE Antennas and Propagation Magazine*, 45(2):13–19, 2003.

[10] Alvin K. Benson. *Great Lives From History.* Number Inventors & inventions in Great Lives From History. Salem Press, 2010.

[11] Dan Hooper. *Dark Cosmos: In Search of Our Universe's Missing Mass and Energy*. HarperCollins e-books, 2006.

[12] Liudmila Nickelson. *Reflection and Transmission of Plane Electromagnetic Waves*. In *Electromagnetic Theory and Plasmonics for Engineers*, pages 363–424. Springer Singapore, Singapore, 2018.

[13] John S. Seybold. *Introduction to RF Propagation*. John Wiley & Sons, Inc., 2005.

[14] International Telecommunication Union. *Effects of building materials and structures on radiowave propagation above about 100 MHz*. https://www.itu.int/rec/R-REC-P.2040/en, 07 2015. Recommendation ITU-R P.2040-1.

[15] P Ali-Rantala, L Ukkonen, L Sydanheimo, M Keskilammi, and M Kivikoski. *Different kinds of walls and their effect on the attenuation of radiowaves indoors*. In *IEEE Antennas and Propagation Society International Symposium. Digest. Held in conjunction with: USNC/CNC/URSI North American Radio Sci. Meeting (Cat. No.03CH37450)*, volume 3, pages 1020–1023 vol.3. IEEE, 2003.

[16] Engineering ToolBox. *Permeability*, 2016. [Online; accessed Nov, 29, 2020] Retrieved from: `https://www.engineeringtoolbox.com/permeability-d_1923.html`.

[17] Atef Z. Elsherbeni and Demir Veysel. *The finite-difference time-domain method for electromagnetics with MATLAB® simulations*. ACES series. SciTech Publishing, Edison, New Jersey, second edition. edition, 2015.

[18] Kane S. Yee. *Numerical Solution of Initial Boundary Value Problems Involving Maxwell's Equations in Isotropic Media. IEEE Transactions on Antennas and Propagation*, 14(3):302–307, 1966.

[19] John B Schneider. *Understanding the Finite-Difference Time-Domain Method*, 2020.

[20] Allen Taflove and Hagness Susan C. *Computational electrodynamics: the finite-difference time-domain method*. Artech House, Inc., 3rd edition, 2005.

[21] Jean-Pierre Berenger. *"A perfectly matched layer for the absorption of electromagnetic waves". Journal of Computational Physics*, 114(2):185 – 200, 1994.

[22] Rakennustieto. *Ulkoseinärakenteita, RT 82-11006*, 10 2010.

[23] Rakennustieto. *Väliseinärakenteita, RT 82-10903*, 09 2007.

Appendix 1. FDTD flowchart

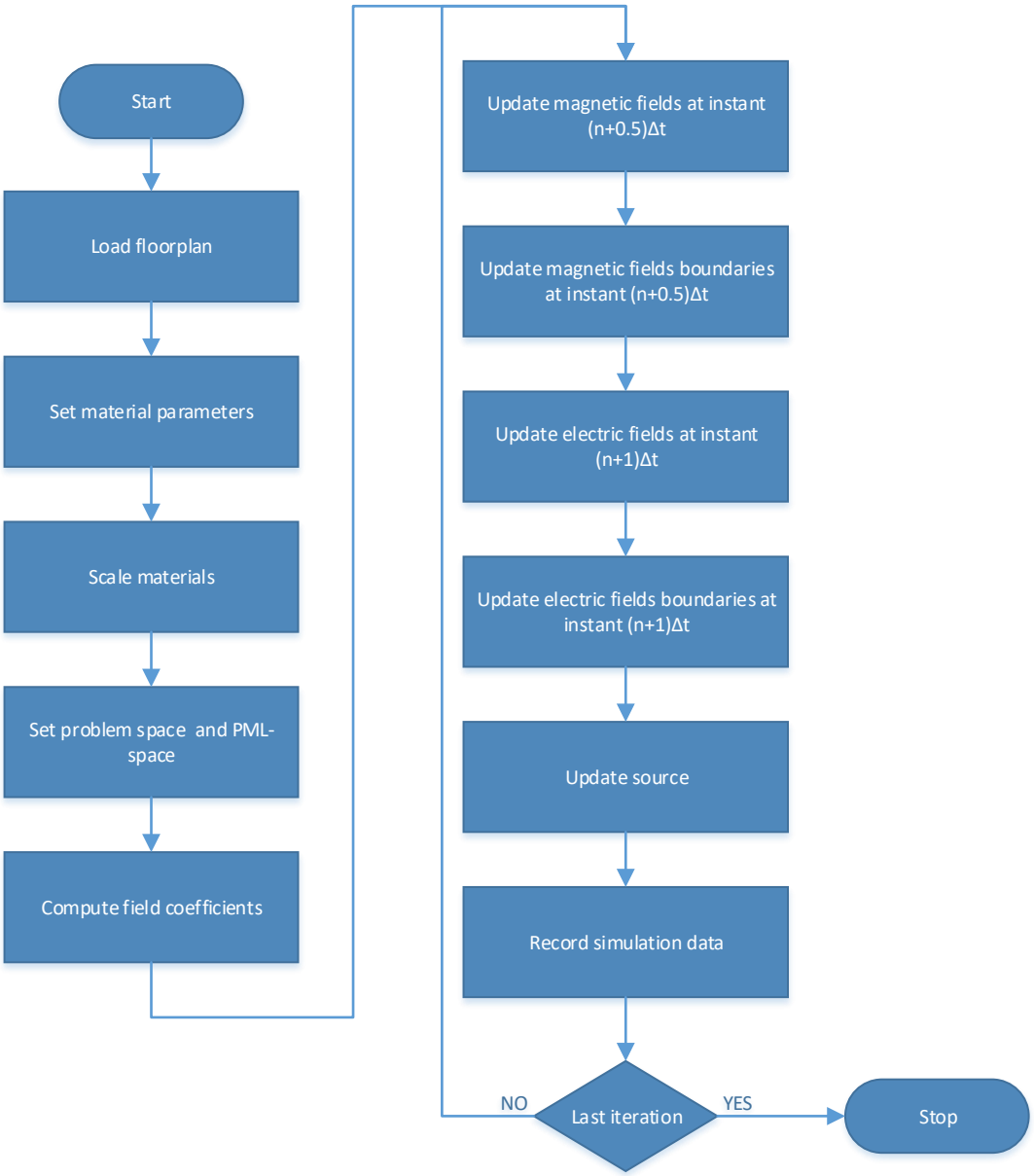

Appendix 2. 3D FDTD update equations

Electric field update equations

$$
\begin{aligned}
E_{\mathrm{x}}^{n+1}(i,j,k) =& C_{\mathrm{exe}}(i,j,k) \times E_{\mathrm{x}}^{n}(i,j,k) \\
&+ C_{\mathrm{exhz}}(i,j,k) \times \left(H_{\mathrm{z}}^{n+\frac{1}{2}}(i,j,k) - H_{\mathrm{z}}^{n+\frac{1}{2}}(i,j-1,k) \right) \\
&+ C_{\mathrm{exhy}}(i,j,k) \times \left(H_{\mathrm{y}}^{n+\frac{1}{2}}(i,j,k) - H_{\mathrm{y}}^{n+\frac{1}{2}}(i,j,k-1) \right) \\
&+ C_{\mathrm{exj}}(i,j,k) \times J_{\mathrm{ix}}^{n+\frac{1}{2}}(i,j,k)
\end{aligned}
$$

where C_{exe}, C_{exhz}, C_{exhy} and C_{exj} are

$$
\begin{aligned}
C_{\mathrm{exe}}(i,j,k) &= \frac{2\varepsilon_{\mathrm{x}}(i,j,k) - \Delta t \sigma_{\mathrm{x}}^{e}(i,j,k)}{2\varepsilon_{\mathrm{x}}(i,j,k) + \Delta t \sigma_{\mathrm{x}}^{e}(i,j,k)} \\
C_{\mathrm{exhz}}(i,j,k) &= \frac{2\Delta t}{\left(2\varepsilon_{\mathrm{x}}(i,j,k) + \Delta t \sigma_{\mathrm{x}}^{e}(i,j,k)\right)\Delta y} \\
C_{\mathrm{exhy}}(i,j,k) &= -\frac{2\Delta t}{\left(2\varepsilon_{\mathrm{x}}(i,j,k) + \Delta t \sigma_{\mathrm{x}}^{e}(i,j,k)\right)\Delta z} \\
C_{\mathrm{exj}}(i,j,k) &= -\frac{2\Delta t}{2\varepsilon_{\mathrm{x}}(i,j,k) + \Delta t \sigma_{\mathrm{x}}^{e}(i,j,k)}
\end{aligned}
$$

$$
\begin{aligned}
E_{\mathrm{y}}^{n+1}(i,j,k) =& C_{\mathrm{eye}}(i,j,k) \times E_{y}^{n}(i,j,k) \\
&+ C_{\mathrm{eyhx}}(i,j,k) \times \left(H_{x}^{n+\frac{1}{2}}(i,j,k) - H_{x}^{n+\frac{1}{2}}(i,j-1,k) \right) \\
&+ C_{\mathrm{eyhz}}(i,j,k) \times \left(H_{z}^{n+\frac{1}{2}}(i,j,k) - H_{z}^{n+\frac{1}{2}}(i,j,k-1) \right) \\
&+ C_{\mathrm{eyj}}(i,j,k) \times J_{iy}^{n+\frac{1}{2}}(i,j,k)
\end{aligned}
$$

Appendix 2. (continued)

where C_{eye}, C_{eyhz}, C_{eyhy} and C_{eyj} are

$$
\begin{aligned}
C_{\text{eye}}(i,j,k) &= \frac{2\varepsilon_{\text{y}}(i,j,k) - \Delta t\sigma^{e}_{\text{y}}(i,j,k)}{2\varepsilon_{\text{y}}(i,j,k) + \Delta t\sigma^{e}_{\text{y}}(i,j,k)} \\
C_{\text{eyhx}}(i,j,k) &= \frac{2\Delta t}{\left(2\varepsilon_{\text{y}}(i,j,k) + \Delta t\sigma^{e}_{\text{y}}(i,j,k)\right)\Delta z} \\
C_{\text{eyhz}}(i,j,k) &= -\frac{2\Delta t}{\left(2\varepsilon_{\text{y}}(i,j,k) + \Delta t\sigma^{e}_{\text{y}}(i,j,k)\right)\Delta x} \\
C_{\text{eyj}}(i,j,k) &= -\frac{2\Delta t}{2\varepsilon_{\text{y}}(i,j,k) + \Delta t\sigma^{e}_{\text{y}}(i,j,k)}
\end{aligned}
$$

$$
\begin{aligned}
E^{n+1}_{\text{z}}(i,j,k) =& C_{\text{eze}}(i,j,k) \times E^{n}_{z}(i,j,k) \\
&+ C_{\text{ezhy}}(i,j,k) \times \left(H^{n+\frac{1}{2}}_{\text{y}}(i,j,k) - H^{n+\frac{1}{2}}_{\text{y}}(i,j-1,k)\right) \\
&+ C_{\text{ezhx}}(i,j,k) \times \left(H^{n+\frac{1}{2}}_{\text{x}}(i,j,k) - H^{n+\frac{1}{2}}_{\text{x}}(i,j,k-1)\right) \\
&+ C_{\text{ezj}}(i,j,k) \times J^{n+\frac{1}{2}}_{iz}(i,j,k)
\end{aligned}
$$

where C_{eze}, C_{ezhy}, C_{ezhx} and C_{ezj} are

$$
\begin{aligned}
C_{\text{eze}}(i,j,k) &= \frac{2\varepsilon_{\text{z}}(i,j,k) - \Delta t\sigma^{e}_{\text{z}}(i,j,k)}{2\varepsilon_{\text{y}}(i,j,k) + \Delta t\sigma^{e}_{\text{y}}(i,j,k)} \\
C_{\text{ezhy}}(i,j,k) &= \frac{2\Delta t}{\left(2\varepsilon_{\text{z}}(i,j,k) + \Delta t\sigma^{e}_{\text{z}}(i,j,k)\right)\Delta x} \\
C_{\text{ezhx}}(i,j,k) &= -\frac{2\Delta t}{\left(2\varepsilon_{\text{z}}(i,j,k) + \Delta t\sigma^{e}_{\text{z}}(i,j,k)\right)\Delta y} \\
C_{\text{ezj}}(i,j,k) &= -\frac{2\Delta t}{2\varepsilon_{\text{z}}(i,j,k) + \Delta t\sigma^{e}_{\text{z}}(i,j,k)}
\end{aligned}
$$

Appendix 2. (continued)

Magnetic field update equations

$$
\begin{aligned}
H_{\mathrm{x}}^{n+\frac{1}{2}}(i,j,k) =& C_{\mathrm{hxh}}(i,j,k) \times H_{\mathrm{x}}^{n-\frac{1}{2}}(i,j,k) \\
&+ C_{\mathrm{hxey}}(i,j,k) \times \left(E_{\mathrm{y}}^{n}(i,j,k+1) - E_{\mathrm{y}}^{n}(i,j,k)\right) \\
&+ C_{\mathrm{hxez}}(i,j,k) \times \left(E_{\mathrm{z}}^{n}(i,j+1,k) - E_{\mathrm{z}}^{n}(i,j,k)\right) \\
&+ C_{\mathrm{hxm}}(i,j,k) \times M_{\mathrm{ix}}^{n}(i,j,k)
\end{aligned}
$$

where C_{hxh}, C_{hxey}, C_{hxez}, and C_{hxm} are

$$
\begin{aligned}
C_{\mathrm{hxh}}(i,j,k) &= \frac{2\mu_x(i,j,k) - \Delta t \sigma_x^m(i,j,k)}{2\mu_x(i,j,k) + \Delta t \sigma_x^m(i,j,k)} \\
C_{\mathrm{hxey}}(i,j,k) &= \frac{2\Delta t}{\left(2\mu_x(i,j,k) + \Delta t \sigma_x^m(i,j,k)\right)\Delta z} \\
C_{\mathrm{hxez}}(i,j,k) &= -\frac{2\Delta t}{\left(2\mu_x(i,j,k) + \Delta t \sigma_x^m(i,j,k)\right)\Delta y} \\
C_{\mathrm{hxm}}(i,j,k) &= -\frac{2\Delta t}{2\mu_x(i,j,k) + \Delta t \sigma_x^m(i,j,k)}
\end{aligned}
$$

$$
\begin{aligned}
H_{\mathrm{y}}^{n+\frac{1}{2}}(i,j,k) =& C_{\mathrm{hyh}}(i,j,k) \times H_{\mathrm{y}}^{n-\frac{1}{2}}(i,j,k) \\
&+ C_{\mathrm{hyez}}(i,j,k) \times \left(E_{\mathrm{z}}^{n}(i,j,k+1) - E_{\mathrm{z}}^{n}(i,j,k)\right) \\
&+ C_{\mathrm{hyex}}(i,j,k) \times \left(E_{\mathrm{x}}^{n}(i,j+1,k) - E_{\mathrm{x}}^{n}(i,j,k)\right) \\
&+ C_{\mathrm{hym}}(i,j,k) \times M_{\mathrm{iy}}^{n}(i,j,k)
\end{aligned}
$$

where C_{hyh}, C_{hyez}, C_{hyex}, and C_{hym} are

$$
\begin{aligned}
C_{\mathrm{hyh}}(i,j,k) &= \frac{2\mu_y(i,j,k) - \Delta t \sigma_y^m(i,j,k)}{2\mu_y(i,j,k) + \Delta t \sigma_y^m(i,j,k)} \\
C_{\mathrm{hyez}}(i,j,k) &= \frac{2\Delta t}{\left(2\mu_y(i,j,k) + \Delta t \sigma_y^m(i,j,k)\right)\Delta x} \\
C_{\mathrm{hyex}}(i,j,k) &= -\frac{2\Delta t}{\left(2\mu_y(i,j,k) + \Delta t \sigma_y^m(i,j,k)\right)\Delta z} \\
C_{\mathrm{hym}}(i,j,k) &= -\frac{2\Delta t}{2\mu_y(i,j,k) + \Delta t \sigma_y^m(i,j,k)}
\end{aligned}
$$

Appendix 2. (continued)

$$
\begin{aligned}
H_{\mathrm{z}}^{n+\frac{1}{2}}(i,j,k) =& C_{\mathrm{hzh}}(i,j,k) \times H_{\mathrm{z}}^{n-\frac{1}{2}}(i,j,k) \\
&+ C_{\mathrm{hzex}}(i,j,k) \times \left(E_{\mathrm{x}}^{n}(i,j,k+1) - E_{\mathrm{x}}^{n}(i,j,k)\right) \\
&+ C_{\mathrm{hzey}}(i,j,k) \times \left(E_{\mathrm{y}}^{n}(i,j+1,k) - E_{\mathrm{y}}^{n}(i,j,k)\right) \\
&+ C_{\mathrm{hzm}}(i,j,k) \times M_{\mathrm{iz}}^{n}(i,j,k)
\end{aligned}
$$

where C_{hzh}, C_{hzex}, C_{hzey}, and C_{hzm} are

$$
\begin{aligned}
C_{\mathrm{hzh}}(i,j,k) &= \frac{2\mu_z(i,j,k) - \Delta t \sigma_z^m(i,j,k)}{2\mu_z(i,j,k) + \Delta t \sigma_z^m(i,j,k)} \\
C_{\mathrm{hzex}}(i,j,k) &= \frac{2\Delta t}{\left(2\mu_z(i,j,k) + \Delta t \sigma_z^m(i,j,k)\right)\Delta y} \\
C_{\mathrm{hzey}}(i,j,k) &= -\frac{2\Delta t}{\left(2\mu_z(i,j,k) + \Delta t \sigma_z^m(i,j,k)\right)\Delta x} \\
C_{\mathrm{hzm}}(i,j,k) &= -\frac{2\Delta t}{2\mu_z(i,j,k) + \Delta t \sigma_z^m(i,j,k)}
\end{aligned}
$$

Appendix 3. 2D FDTD transverse modes

Transverse electric mode

$$\begin{aligned} H_{\mathrm{z}}^{n+\frac{1}{2}}(i,j) =& C_{\mathrm{hzh}}(i,j) \times H_{\mathrm{z}}^{n-\frac{1}{2}}(i,j) \\ &+ C_{\mathrm{hzex}}(i,j) \times \left(E_{\mathrm{x}}^{n}(i,j+1) - E_{\mathrm{x}}^{n}(i,j)\right) \\ &+ C_{\mathrm{hzey}}(i,j) \times \left(E_{\mathrm{y}}^{n}(i+1,j) - E_{\mathrm{y}}^{n}(i,j)\right) \\ &+ C_{\mathrm{hzm}}(i,j) \times M_{\mathrm{iz}}^{n}(i,j) \end{aligned}$$

where C_{hzh}, C_{hzex}, C_{hzey}, and C_{hzm} are

$$\begin{aligned} C_{\mathrm{hzh}}(i,j) &= \frac{2\mu_z(i,j) - \Delta t \sigma_z^m(i,j)}{2\mu_z(i,j) + \Delta t \sigma_z^m(i,j)} \\ C_{\mathrm{hzex}}(i,j) &= \frac{2\Delta t}{\left(2\mu_z(i,j) + \Delta t \sigma_z^m(i,j)\right)\Delta y} \\ C_{\mathrm{hzey}}(i,j) &= -\frac{2\Delta t}{\left(2\mu_z(i,j) + \Delta t \sigma_z^m(i,j)\right)\Delta x} \\ C_{\mathrm{hzm}}(i,j) &= -\frac{2\Delta t}{2\mu_z(i,j) + \Delta t \sigma_z^m(i,j)} \end{aligned}$$

$$\begin{aligned} E_{\mathrm{x}}^{n+1}(i,j) =& C_{\mathrm{exe}}(i,j) \times E_{\mathrm{x}}^{n}(i,j) \\ &+ C_{\mathrm{exhz}}(i,j) \times \left(H_{\mathrm{z}}^{n+\frac{1}{2}}(i,j) - H_{\mathrm{z}}^{n+\frac{1}{2}}(i,j-1)\right) \\ &+ C_{\mathrm{exj}}(i,j) \times J_{\mathrm{ix}}^{n+\frac{1}{2}}(i,j) \end{aligned}$$

where C_{exe}, C_{exhz} and C_{exj} are

$$\begin{aligned} C_{\mathrm{exe}}(i,j) &= \frac{2\varepsilon_{\mathrm{x}}(i,j) - \Delta t \sigma_{\mathrm{x}}^e(i,j)}{2\varepsilon_{\mathrm{x}}(i,j) + \Delta t \sigma_{\mathrm{x}}^e(i,j)} \\ C_{\mathrm{exhz}}(i,j) &= \frac{2\Delta t}{\left(2\varepsilon_{\mathrm{x}}(i,j) + \Delta t \sigma_{\mathrm{x}}^e(i,j)\right)\Delta y} \\ C_{\mathrm{exj}}(i,j) &= -\frac{2\Delta t}{2\varepsilon_{\mathrm{x}}(i,j) + \Delta t \sigma_{\mathrm{x}}^e(i,j)} \end{aligned}$$

Appendix 3. (continued)

$$
\begin{aligned}
E_{\mathrm{y}}^{n+1}(i,j) =& C_{\mathrm{eye}}(i,j) \times E_{y}^{n}(i,j) \\
&+ C_{\mathrm{eyhz}}(i,j) \times \left(H_{z}^{n+\frac{1}{2}}(i,j) - H_{z}^{n+\frac{1}{2}}(i,j-1) \right) \\
&+ C_{\mathrm{eyj}}(i,j) \times J_{iy}^{n+\frac{1}{2}}(i,j)
\end{aligned}
$$

where C_{eye}, C_{eyhz}, C_{eyhy} and C_{eyj} are

$$
\begin{aligned}
C_{\mathrm{eye}}(i,j) &= \frac{2\varepsilon_{\mathrm{y}}(i,j) - \Delta t \sigma_{\mathrm{y}}^{e}(i,j)}{2\varepsilon_{\mathrm{y}}(i,j) + \Delta t \sigma_{\mathrm{y}}^{e}(i,j)} \\
C_{\mathrm{eyhz}}(i,j) &= -\frac{2\Delta t}{\left(2\varepsilon_{\mathrm{y}}(i,j) + \Delta t \sigma_{\mathrm{y}}^{e}(i,j)\right) \Delta x} \\
C_{\mathrm{eyj}}(i,j) &= -\frac{2\Delta t}{2\varepsilon_{\mathrm{y}}(i,j) + \Delta t \sigma_{\mathrm{y}}^{e}(i,j)}
\end{aligned}
$$

Appendix 3. (continued)

Transverse magnetic mode

$$\begin{aligned} E_{\mathrm{z}}^{n+1}(i,j) =& C_{\mathrm{eze}}(i,j) \times E_z^n(i,j) \\ &+ C_{\mathrm{ezhy}}(i,j) \times \left(H_{\mathrm{y}}^{n+\frac{1}{2}}(i,j) - H_{\mathrm{y}}^{n+\frac{1}{2}}(i-1,j) \right) \\ &+ C_{\mathrm{ezhx}}(i,j) \times \left(H_{\mathrm{x}}^{n+\frac{1}{2}}(i,j) - H_{\mathrm{x}}^{n+\frac{1}{2}}(i,j-1) \right) \\ &+ C_{\mathrm{ezj}}(i,j) \times J_{iz}^{n+\frac{1}{2}}(i,j) \end{aligned}$$

where C_{eze}, C_{ezhy}, C_{ezhx} and C_{ezj} are

$$\begin{aligned} C_{\mathrm{eze}}(i,j) &= \frac{2\varepsilon_{\mathrm{z}}(i,j) - \Delta t \sigma_{\mathrm{z}}^e(i,j)}{2\varepsilon_{\mathrm{y}}(i,j) + \Delta t \sigma_{\mathrm{y}}^e(i,j)} \\ C_{\mathrm{ezhy}}(i,j) &= \frac{2\Delta t}{\left(2\varepsilon_{\mathrm{z}}(i,j) + \Delta t \sigma_{\mathrm{z}}^e(i,j)\right) \Delta x} \\ C_{\mathrm{ezhx}}(i,j) &= -\frac{2\Delta t}{\left(2\varepsilon_{\mathrm{z}}(i,j) + \Delta t \sigma_{\mathrm{z}}^e(i,j)\right) \Delta y} \\ C_{\mathrm{ezj}}(i,j) &= -\frac{2\Delta t}{2\varepsilon_{\mathrm{z}}(i,j) + \Delta t \sigma_{\mathrm{z}}^e(i,j)} \end{aligned}$$

$$\begin{aligned} H_{\mathrm{x}}^{n+\frac{1}{2}}(i,j) =& C_{\mathrm{hxh}}(i,j) \times H_{\mathrm{x}}^{n-\frac{1}{2}}(i,j) \\ &+ C_{\mathrm{hxez}}(i,j) \times \left(E_{\mathrm{z}}^n(i,j+1) - E_{\mathrm{z}}^n(i,j) \right) \\ &+ C_{\mathrm{hxm}}(i,j) \times M_{\mathrm{ix}}^n(i,j) \end{aligned}$$

where C_{hxh}, C_{hxey}, C_{hxez}, and C_{hxm} are

$$\begin{aligned} C_{\mathrm{hxh}}(i,j) &= \frac{2\mu_x(i,j) - \Delta t \sigma_x^m(i,j)}{2\mu_x(i,j) + \Delta t \sigma_x^m(i,j)} \\ C_{\mathrm{hxez}}(i,j) &= -\frac{2\Delta t}{\left(2\mu_x(i,j) + \Delta t \sigma_x^m(i,j)\right) \Delta y} \\ C_{\mathrm{hxm}}(i,j) &= -\frac{2\Delta t}{2\mu_x(i,j) + \Delta t \sigma_x^m(i,j)} \end{aligned}$$

Appendix 3. (continued)

$$
\begin{aligned}
H_{\mathrm{y}}^{n+\frac{1}{2}}(i,j) =& C_{\mathrm{hyh}}(i,j) \times H_{\mathrm{y}}^{n-\frac{1}{2}}(i,j) \\
&+ C_{\mathrm{hyez}}(i,j) \times \left(E_{\mathrm{z}}^{n}(i+1,j) - E_{\mathrm{z}}^{n}(i,j)\right) \\
&+ C_{\mathrm{hym}}(i,j) \times M_{\mathrm{iy}}^{n}(i,j)
\end{aligned}
$$

where C_{hyh}, C_{hyez}, C_{hyex}, and C_{hym} are

$$
\begin{aligned}
C_{\mathrm{hyh}}(i,j) &= \frac{2\mu_y(i,j) - \Delta t \sigma_y^m(i,j)}{2\mu_y(i,j) + \Delta t \sigma_y^m(i,j)} \\
C_{\mathrm{hyez}}(i,j) &= \frac{2\Delta t}{\left(2\mu_y(i,j) + \Delta t \sigma_y^m(i,j)\right)\Delta x} \\
C_{\mathrm{hym}}(i,j) &= -\frac{2\Delta t}{2\mu_y(i,j) + \Delta t \sigma_y^m(i,j)}
\end{aligned}
$$